University of Alberta

NORMAL AND PATHOLOGICAL DEVELOPMENT OF THE RODENT PRIMORDIAL DIAPHRAGM

by

Darine Abou Marak Dit Roum

A thesis submitted to the Faculty of Graduate Studies and Research
in partial fulfillment of the requirements for the degree of

Master of Science

Department of Physiology

Spring 2011
Edmonton, Alberta

ABSTRACT

The focus of this thesis work was toward advancing our understanding of the normal and pathological development of the diaphragm. This included: (1) studies of the embryology of the primordial diaphragm tissue, the pleuroperitoneal fold (PPF), as it relates to congenital diaphragmatic hernia (CDH), and (2) investigating the relationship between migrating Schwann cells, phrenic axons and muscle cells in the developing diaphragm.

The primary method of investigation was immunolabeling of the phrenic nerve, Schwann cells, muscle cells and the amuscular cellular component of the PPF and the diaphragm using the nitrofen model of CDH and transgenic mouse models.

Together, these data provide the foundation for novel directions of research into CDH pathogenesis and specifically advance our understanding of: (1) the mechanism of CDH pathogenesis with special focus on PPF mesenchymal cells; and (2) the mechanism of axonal guidance and intramuscular branching.

ACKNOWLEDGEMENTS

Special thanks to Dr. John Greer, my supervisor, for giving me the opportunity to work in his lab and providing me with all the support, encouragement and guidance throughout my studies. My time in the lab was a great learning experience.

I would like to thank Dr. Robin Clugston for teaching me all the techniques and for all his advice and help when needed.

I would also like to thank all the members of the Greer Lab: Wei Zhang, Dr. Jun Ren and his wife Xiu, and Floriane Lenal. Their advice and assistance on many occasions was very valuable.

Finally, I would like to thank my Committee members: Dr. Greg Funk, Dr. Simon Gosgnach and Dr. Alan Underhill for their support.

Table of Contents

LIST OF TABLES

LIST OF FIGURES

LIST OF ABBREVIATIONS

AChR	Acetylcholine receptor
ADH	Alcohol dehydrogenase
aCGH	Array-based comparative genomic hybridization
β-gal	β-galactosidase
BPCA	4-Biphenyl carboxylic acid
BrdU	Bromodeoxyuridine
CDH	Congenital diaphragmatic hernia
COUP-TFII	Chicken ovalbumin upstream promoter transcription factorII
CRABP	Cellular retinoic acid binding protein
CRBP	Cellular retinol binding protein
CRL	Crown-rump length
DAB	3,3- Diaminobenzidine tetrahydrochloride
DCC	Deleted in colrectal cancer
DNA	Deoxyribonucleic acid
E	Embryonic day (when followed by a number)
ECMO	Extra-corporeal membrane oxygenation
EMT	Epithelial-mesenchymal transition
EPDC	Epicardial derived cells
hES	Human embryonic stem
LRAT	Lecithin: retinol acyltransferase
MPCs	Muscle precursor cells
MuSK	Muscle specific-kinase
NCAM	Neural cell adhesion molecule
NMJ	Neuromuscular junction
NRG	Neuregulin

PBS	Phosphate buffered saline
PCD	Programmed cell death
PSA-NCAM	Polysialylated neural cell adhesion molecule
PFA	Paraformaldehyde
PPF	Pleuroperitoneal fold
RA	Retinoic acid
RALDH	Retinal dehydrogenase
RAR	Retinoic acid receptor
RARE	Retinoic acid response element
RBP	Retinol binding protein
RNA	Ribonucleic acid
RPE	Retinal pigment epithelial
RPTP	Receptor tyrosine phosphatases
RXR	Retinoid X receptor
SEM	Standard error of the mean
TH	Thyroid hormone
THR	Thyroid hormone receptor
TRE	Thyroid response element
TUNEL	Terminal uridine deoxynucleotidyl transferase dUTP nick end-labeling
WT1	Wilms Tumor

Note – The following convention for abbreviating genes and proteins has been used in this thesis. Human genes are written in capital letters and in italics (*GENE*), human proteins are written in capital letters, but are not italicized (PROTEIN). Rodent genes are written in italics, but only the first

letter is capitalized (*Gene*). Rodent proteins are not italicized and only the first letter is capitalized (Protein).

CHAPTER 1. INTRODUCTION AND LITERATURE REVIEW

1.1 Objectives

General overview: The work described in this thesis is divided into two parts. The first general aim was to improve our understanding of primordial diaphragm development with a focus on the stage most relevant to the pathogenesis of congenital diaphragmatic hernia (CDH). The second aspect expanded upon previous work on diaphragm embryogenesis by examining unresolved questions pertaining to the interactions of migrating phrenic axons, primordial Schwann cells and muscle precursors.

Previous data from multiple rodent CDH models in conjunction with analysis of postmortem human diaphragms from CDH cases, strongly suggests that the initial diaphragmatic defect originates with the formation of the primordial diaphragmatic tissue, the pleuroperitoneal fold (PPF). Specifically, it appears that there may be a defect in the non-muscle component of the PPF. To date, very little is known about the embryogenesis of the various cell types within PPF and how they relate to CDH pathogenesis. The main objectives of the first part of my thesis are to: (1) examine the embryogenesis of the rat PPF from embryonic day (E) 12 when it first emerges from the lateral body wall through to E14 when it is fully formed with a special emphasis on the arrangement of mesenchymal cells; (2) test whether those cells originate from the mesoderm; (3) and test the hypothesis that the pathogenesis of CDH is associated with a reduced number of

mesenchymal cells and the aggregation of muscle precursor cells in the PPF and defective diaphragm.

Our laboratory has been studying the basic mechanisms associated with phrenic nerve and diaphragm embryogenesis. In the broader context of developmental biology, the phrenic nerve-diaphragm system has characteristics that make it an excellent model for studying mammalian nerve-muscle functional unit, including the fact that it is anatomically localized from other striated muscles, and receives efferent innervation from a single nerve (e.g. compared to the limb where many embryonic muscles and nerves are co-mingled). I used transgenic mouse models in the second part of my thesis to examine hypotheses: (1) that Schwann cells lead the migrating phrenic axons toward the PPF and during the process of intramuscular branching; and (2) phrenic axon migration and intramuscular branching is abnormal in the absence of migrating muscle cell precursors.

Chapter 1 is a general introduction providing the necessary background regarding the etiology and pathogenesis of CDH, followed by a description of diaphragm embryogenesis. This provides the basis for understanding the significance of my research and its contribution to the field of CDH and some basic principles associated with mammalian nerve-muscle development.

Chapter 2 is the methods section outlining techniques used to reach the results which are discussed in chapter 3. Chapter 4 is a general discussion and outlines future studies that would extend upon my contributions.

INTRODUCTION

1.2 Diaphragm Anatomy and Function

As far back as 300 million years ago, vertebrates had a primitive amuscular diaphragm that served as a barrier between an upper feeding compartment and a lower digestive tract [reviewed in 47]. The lungs were positioned caudal to the diaphragm in dinosaurs and other reptile and amphibious species [reviewed in 47]. As warm-blooded mammals evolved, the lungs became positioned rostral to the diaphragm [reviewed in 47]. Through evolution, the diaphragm became muscularized and is the primary muscle controlling ribcage expansion and lung inflation and is present in all mammalian species examined [reviewed in 47].

The word diaphragm is derived from the Greek *dia* (in between) and *phragma* (fence) [reviewed in 47]. The diaphragm is a musculo-fibrous dome-shaped membrane between the thoracic and abdominal cavities [reviewed in 47]. In humans, the diaphragm develops between 4 and 10 weeks of gestation and in mice between E10.5 and E15.5 (gestation= 18.5 days) [reviewed in: 1; 39]. It has a similar characteristic appearance in both humans and rodents, prominently muscularized peripherally and a fibrous, non-muscularized central tendon which remains attached to the liver by the falciform and coronary ligaments [reviewed in: 1; 47]. In addition, it has three major openings: the caval opening for the inferior vena cava, the esophageal hiatus for the esophagus, and the

aortic hiatus through which the aorta, the thoracic duct and the azygos vein pass [reviewed in: 1; 47].

In mammals, the diaphragm serves two very important functions. First, it is the primary respiratory muscle. During inhalation, the diaphragm contracts and thereby induces the expansion of the thoracic cavity, creating a negative intrathoracic pressure to help air move into the lungs. In contrast, on exhalation the diaphragm relaxes to allow air to be drawn out passively from the lungs by elastic recoil. Second, the diaphragm forms a physical barrier between the thoracic and abdominal cavities to prevent the abdominal organs from moving into the thorax [reviewed in: 15, 39]. It is this latter function which is impaired in CDH during early embryologic development and, because of this defect, the viscera move into the chest cavity, impeding the development of the lungs and resulting in pulmonary hypoplasia (figure 1.1) [reviewed in: 15, 39, 47].

Other non-respiratory functions of the diaphragm include: helping to expel vomit, feces, and urine from the body through increasing intra-abdominal pressure and preventing acid reflux through exerting pressure on the lower esophageal sphincter [reviewed in 47].

1.3 Congenital Diaphragmatic Hernia (CDH)

1.3.1 Clinical Aspects

CDH remains the most life-threatening cause of severe respiratory

failure in term infants [reviewed in 56]. Its incidence is approximately 1 in 2500 live births and accounts for ~ 8% of all major congenital anomalies [reviewed in: 16, 56]. Phenotypically, CDH can be characterized into subtypes based on the location or nature of the defect [reviewed in 15]. In humans, there are four principle types of hernias: a posterolateral Bochdalek-type (greater than 95% of the cases), an anterior Morgagni-type, a central tendon hernia, and eventration of the diaphragm [reviewed in: 15, 16, 84]. Eighty-five percent of the major Bochdalek-type hernias occur on the left side, 13% on the right side, and only 2% are bilateral [reviewed in 84].

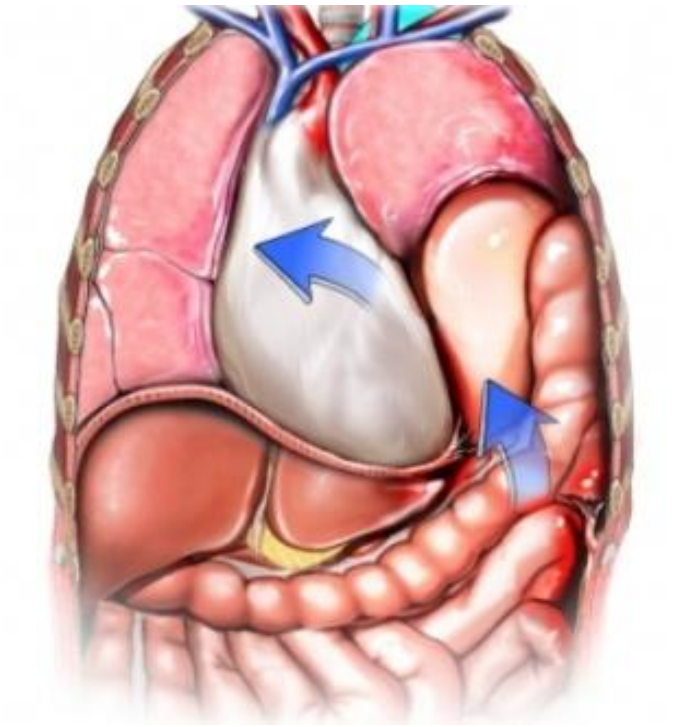

Figure 1.1 Congenital Diaphragmatic Hernia (CDH).

Ventral view showing abdominal contents herniating into the thorax through a hole in the left diaphragm causing lung hypoplasia [Adapted from 2009 Nucleus Medical media, Inc.] .

CDH occurs as an isolated birth defect (isolated CDH) with a mortality rate ranging from 20 to 60 % mainly due to differences in case selection, or is associated with additional malformations (non-isolated CDH) including congenital heart disease, abnormalities of the central nervous system and urogenital anomalies with a mortality rate as high as 90% [reviewed in: 25, 55, 84; 27]. Several predictors of mortality include early prenatal diagnosis, polyhydramnions, presence of associated anomalies, right-sided diaphragmatic hernia, intrathoracic stomach and/or liver, low lung-to-head ratio and low Apgar scores [reviewed in 25].

Postnatal treatment strategies include nitric oxide administration, high-frequency oscillatory ventilation, exogenous surfactant administration and extracoporeal membrane oxygenation (ECMO) with limited impact on prognosis and considerable morbidity among survivors [reviewed in: 28, 55, 84]. Prenatal treatments have also been attempted in CDH such as open fetal diaphragmatic repair and fetoscopic tracheal occlusion with the survival benefit being questionable [reviewed in: 28, 55, 84]. Total acute-care costs are estimated to be ~ $350,000 per patient. Further, the problem with these new treatment modalities is that they are designed for treating the sequelae of CDH, replacing mortality with a higher morbidity due to the absence of sufficient lung protective strategies [reviewed in: 28, 84]. Towards improving prenatal screening, treatment, or reducing the incidence of this anomaly, it will be important to better understand the etiology and pathogenesis of CDH [reviewed in: 55, 84].

1.3.2 Surgical Models of CDH

Surgical models are based on the surgical creation of a diaphragmatic defect most commonly in sheep and rabbits relatively late in gestation [reviewed in: 39, 84]. In sheep, the hernia is created at gestational days 72-75 (term is 145-149 days), equivalent to gestational age 10 weeks in humans, with the abdominal bowel positioned into the chest to optimally mimic that aspect of human CDH. This corresponds to pseudoglandular stage of lung development and the moment of pleuroperitoneal canal fusion during diaphragmatic development [reviewed in 39]. Later, rabbits were used as a surgical model because of its shorter gestational period (term is 31 days with the hernia created at day 23), larger litter size, easy availability and reduced relative cost [reviewed in 39].

The surgical models were especially suitable to investigate interventional therapies in CDH such as administration of corticosteroids, in utero repair of diaphragmatic defect and prenatal induction of pulmonary growth by tracheal occlusion [reviewed in: 39, 84]. However, the disadvantage of the surgical models is that the diaphragmatic defect is created relatively late, following substantial normal lung and diaphragm development [reviewed in: 39, 84].

As a result, to better understand and study the etiology and pathogenesis of CDH, rat dietary, teratogenic and recently genetic mouse models of CDH have been introduced. The various models and potential overlapping mechanisms of actions between the models are discussed below.

1.3.3 Etiology of CDH

A- Retinoid Hypothesis of CDH Etiology

Vitamin A nutrition is essential during embryonic development as noted by early nutritionists who observed fetal death or congenital abnormalities in the offspring of mothers with insufficient vitamin A uptake during pregnancy [reviewed in 90]. All retinoids, vitamin A and its metabolites, are obtained from the diet either as a preformed retinoid (primarily as a dietary retinol or retinyl ester) in animal meat or as pro-retinoid carotenoid ester (primarily as β-carotene) in vegetables [reviewed in: 25, 41]. Retinoids serve an important function in several biological processes such as cellular growth, proliferation, differentiation, reproduction and morphogenesis [82].

In enterocytes, these dietary retinoids are then processed and packaged with other dietary lipids as retinyl esters into chylomicrons by the enzyme lecithin: retinol acyltransferase (LRAT) [reviewed in 41]. Most of the dietary retinoid is stored as retinyl ester in the stellate cells of the liver but may also be found in the lung during embryonic life [reviewed in: 25, 41]. These hepatic stores can then be mobilized into the circulation as retinol bound to plasma retinol binding protein (RBP) which is itself complexed with transthyretin [reviewed in: 25, 41]. Distal tissues acquire retinol from the circulating retinal-RBP complex or post-prandially from chylomicrons and oxidize it enzymatically [reviewed in 41]. At the cellular level of these target tissues, retinol binds to cellular retinol binding proteins (CRBP1 and 2) and stored either as retinyl esters or converted into retineldyde (retinal) by

cytosolic alcohol dehydrogenases (ADH) and ultimately into retinoic acid (RA) by an irreversible oxidative reaction via retinaldehyde dehydrogenases (RALDHs) and in particular RALDH2 which is considered the main enzyme in regulating RA synthesis [reviewed in: 25, 41]. RA signal transduction is mediated by binding of ligand to its cognate receptors which drive expression of retinoic-acid responsive genes. There are two families of nuclear receptors: retinoic acid receptors (RARs) with 3 different isotypes α, β and γ, activated by both all-trans and 9-cis RA, and retinoid X receptors (RXRs), including α, β and γ, activated only by 9-cis RA. RARs and RXRs are both members of the steroid/thyroid hormone superfamily of ligand-inducible transcriptional regulators [reviewed in 25; 82]. RARs seem to operate only as heterodimeric RAR/RXR. RXRs can also act either as homodimers or heterodimers enhancing the binding of RARs, vitamin-D3 receptors and thyroid hormone receptor, to their responsive elements [reviewed in 25; 82]. The RAR/RXR complex then binds to a specific DNA sequences called retinoid responsive elements (RARE and RXRE respectively) usually upstream of retinoid regulated genes [reviewed in 25; 82].

The "retinoid hypothesis" of CDH etiology was based on animal and human data [9; 17; 48] showing a correlation between diaphragmatic hernia and:

(1) Vitamin A deficiency

(2) Retinoid receptor double null mutant mice

(3) Exposure to teratogens that interfere with RA synthesis

(4) The expression pattern of the components necessary for RA synthesis and signaling within the diaphragm

(5) Pilot study showing abnormal retinoid homeostasis in human newborns with CDH

One of the first pieces of evidence linking retinoids with CDH was published in 1946, whereby some off-spring of vitamin A deficient dams revealed many congenital anomalies such as underdeveloped lungs, incomplete pleural chambers around the pericardial cavity, spongy heart muscle, hypoplastic kidneys and diaphragmatic hernia with a possible protrusion of the liver into the thoracic cavity [85].

In 1994 Mendelshon et al. reported posterolateral diaphragmatic hernia in a subset of αβ2 and one out of four $\alpha\beta2^{+/-}$ double mutant mice in conjunction with lung hypoplasia, heart and urogenital defects [52; reviewed in 55; 61].

The most common teratogenic model of CDH in rodents, used for the past two decades to investigate CDH anomalies is the nitrofen model [61; reviewed in 84]. Nitrofen (2,4-dichlorophenyl- *p* -nitrophenyl ether), is a diphenyl ether originally used as a herbicide [40; reviewed in 84]. Although administration of a single dose of nitrofen during mid-gestation, typically between E8 and 10 had no apparent affect on pregnant dams, it did cause developmental anomalies in their embryos including diaphragmatic hernia which were similar in location and extent to human CDH and associated pulmonary hypoplasia, pulmonary hypertension, cardiovascular and skeletal defects [15;

20; reviewed in 84].

Several hypotheses have been put forward to explain the possible teratogenic effects of nitrofen [64]. Initially, based on its structural similarity with thyroid hormone (TH), nitrofen was suggested to cause CDH by altering TH levels and thyroid hormone receptor (THR) functions [40, 64]. However, studies of the direct impact of nitrofen on thyroid hormone signaling were ultimately inconclusive suggesting an alternative mode of action [40]. Nitrofen did not antagonize THR action at the administered levels, nor did it cause a perturbation of the thyroid response element (TRE) action or there was a reduction in the incidence of CDH when nitrofen was administered with TH [40; 64].

Subsequently, it was discovered that nitrofen caused a decline in β-galactosidase activity of RARE-LacZ genetically modified mice and there was a reduction in the incidence of CDH and increased lung growth following Vitamin A administration in the nitrofen rat model [13; 40; 56; 61; 80]. Recently, a study by Noble et al. using *in vitro* cell assays in conjunction with whole animal rodent models confirmed nitrofen-induced suppression of RALDH2 activity rather than expression [40; 64]. Three other CDH-inducing teratogens have been identified: 4-biphenyl carboxylic acid (BPCA), bisdiamine [N, N-octamethylenebis (dichloroacetamide)], and SB-210661. BPCA is a breakdown product of a thromboxane-A2 receptor antagonist, bisdiamine is a spermatogenesis inhibitor, and SB-210661 is a benzofuranyl urea derivative developed for inhibiting 5-lipoxygenase. These drugs have similar chemical

structures to each other and to nitrofen, and also induce CDH in rats by RALDH2 inhibition [15; 53].

Recently, Clugston et al. demonstrated the expression of proteins necessary for RA synthesis from retinal, transport to the nucleus and signal transduction via its nuclear receptors within the primordial diaphragm [17]. The study showed a wide expression of CRABPII (cellular retinoic acid binding protein II), RALDH2, RARα, RARγ and RXRα. The expression of RARα within the PPF was of particular interested because of its location in mesenchymal cells of the dorsolateral region typically affected in CDH primordial diaphragm cells [17].

Two clinical studies further support the link between vitamin A deficiency and CDH previously noted in experimental animals. In the first study, the plasma retinol and RBP levels were 50% less in the CDH newborns compared to the control, while retinol levels of CDH mothers were higher than control mothers [48]. Recently, a second larger study confirmed lower levels of retinol and RBP in CDH newborns, but there was no difference in retinol and RBP between CDH and control mothers [9]. These clinical studies suggest that there may be: (1) disturbed fetal vitamin A signaling due to defective receptors, converting enzymes, binding proteins in the embryo during early gestation, or (2) impaired retinol transport from the yolk sac to the fetus [9; 48].

An alternative hypothesis of nitrofen teratogenic mode of action “the apoptosis hypothesis” suggests nitrofen-induced apoptosis of

undifferentiated cells. This is supported by an observation of excessive cell death in the presomitic mesenchyme surrounding cervical somites 2, 3 and 4 of fetal rats and increased caspase-3 activities and DNA fragmentation in multiple teratocarcinoma cell lines [5; 40]. However, no evidence of apoptosis in the developing diaphragm tissue in any of the rodent CDH models has been reported.

B- Genetic Etiology of CDH

In addition to the recently proposed "retinoid hypothesis", the genetic origins of CDH are of significant interest, largely due to the characterization of mutant mice with abnormal diaphragm phenotypes and genetic screening in infants with CDH [19]. Chromosomal abnormalities were identified in 10-20% of CDH cases with a higher rate in cases with associated malformations [reviewed in 27]. The existence of so-called CDH-critical regions, parts of chromosomes where recurring structural abnormalities have been found in multiple cases, suggest the presence of genes that cause or predispose one to the development of CDH [19; reviewed in 27]. Several techniques have been used to identify chromosome abnormalities including R- and G-banded analysis, FISH and most recently array-based comparative genomic hybridization (aCGH) [reviewed in 27]. In addition, genetic studies using knockout mice have begun to shed light on the function of genes linked to CDH by making the gene of interest inoperable [reviewed in 40, 84].

The first and best characterized critical region to be identified is

located at 15q26, the deletion of which account for ~ 1.5% of CDH cases and is associated with very high mortality [reviewed in 19]. *COUP-TFII* (Chicken ovalbumin upstream promoter transcription-factor II) is one of the four known genes residing within this critical region [reviewed in 1; 21; 87]. It is a member of the steroid/thyroid hormone receptor superfamily with an important role in embryonic development. It is expressed in the lung, the foregut mesenchyme, the primordial diaphragm and the septum transversum [21, 87]. *Coup-tfII* null mice die prior to diaphragmatic embryogenesis due to many malformations including defects in angiogenesis, heart development, and renal malformations [reviewed in 1; 21; 87]. However, *Nkx3-2 Cre*-induced *Coup-tfII* conditional null deletions restricted to the foregut mesenchyme survive to later stages and exhibit Bochdalek type CDH, the most common form of CDH [reviewed in 1; 21; 87].

Similar to *Coup-tfII*, *Wt1* null mice also demonstrate a Bochdalek hernia phenotype and Wt1 expression is required for the development of the genitourinary system, the spleen, the heart and the diaphragm [reviewed in 1, 84]. However, besides a few reports of mutations of *WT1* (Wilms' Tumor-1) in human case reports on syndromic CDH such as WAGR and Denys Drash, no relationship between the presence of the *WT1* mutation and isolated CDH was found [reviewed in 84].

Several other regions of the human genome have been identified as putative CDH-critical regions including 8p23.1 and 8q22-23 which harbor *GATA4* and *FOG2* respectively [19]. FOG2 is a transcription cofactor for the

GATA family of transcription factors. Its interaction *in vivo* with GATA4 is essential for normal development of the lungs, heart, diaphragm and gonads [reviewed in 1]. Fog2 is expressed in mesodermal tissues including the mesothelium and primordial diaphragm [reviewed in 1]. There has been a case report of an infant with a specific mutation in the *FOG2* gene and who suffered from diaphragmatic eventration [reviewed in 1; 19]. Furthermore, although *Fog2* null mice die from cardiac defects prior to diaphragm development, mice with a homozygous hypomorphic mutation in *Fog2* have posterior membranous diaphragms and an abnormal pattern of muscularization [reviewed in 1; 19]. Similarly, *Gata4* heterozygous mice have many developmental defects such as midline diaphragmatic hernia and cardiac malformations [37].

1.3.4 Pathogenesis of CDH

Although the mechanisms underlying the pathogenesis of CDH are not fully resolved, there are a number of theories pertaining to the pathogenesis of the disease:

(1) Diaphragm tissue malformation secondary to mal-development of the adjacent lung tissue

(2) Failure of pleuroperitoneal canal closure (i.e. fusion of the primordial diaphragm with the body wall): most commonly cited hypothesis in text-books

(3) Diaphragmatic muscle malformation due to a perturbation of the

normal innervation of the diaphragm by the phrenic nerve

(4) Improper myotube formation within the region of diaphragmatic hernia [4; reviewed in 28]

Theory (1): Central to this hypothesis is that the primordial diaphragm is regulated or influenced directly by the development of the adjacent lung tissue [7]. This notion is not supported for two important reasons. First, Kluth et al. concluded based on visual inspection with scanning electron microscopy, that the lungs were normal prior to invasion of the abdominal contents into the thoracic cavity [42]. Second, in *Fgf10* ($^{-}/^{-}$) null mutant mice that do not develop lung tissue, the diaphragm forms normally and nitrofen induces CDH without any necessary signaling from the lung [8].

Theory (2): Is not supported due to the fact that the diaphragmatic hernia often occur medial to the pleuroperitoneal canals, a pair of narrow channels in the dorsolateral region of the developing diaphragm connecting the peritoneal and pleural cavities, and prior to closure of the left and right pleuroperitoneal canals in all rodent models studied [3].

Theory (3): A study by Allan and Greer [4] demonstrated that prior to naturally occurring programmed cell death (PCD) (E15-E16), the numbers of phrenic motoneurons and axons in CDH rats were similar to those in control rats on both ipsi- and contralateral sides of the hernia, whereas post E16 a large reduction in the number of phrenic motoneurons was observed on the ipsilateral side, in animals with large diaphragmatic hernia [4]. This can be explained by the fact that the number of neuronal cell axons and bodies that

remain after PCD is determined by the target tissue which is malformed in CDH [4].

Theory (4): This hypothesis suggests that myotubes in the region of the hernia are structurally weak due to an abnormality in density and/or distribution, and thus rupture in response to the pressure of the growing abdominal contents and the shear forces associated with the diaphragmatic contractions *in utero* [4]. However, Allan and Greer demonstrated enhanced thickening around the defect most likely being due to the aggregation of muscle precursor cells in the region of the hernia that would normally spread out to populate the entire diaphragm [4].

Collectively, the above data support the idea that the initial defect can be traced back to a malformation of the primordial diaphragmatic anlage, the PPF. In fact, Iritani and Kluth demonstrated a nitrofen-induced defect as early as E13-E14 in the PPF area [reviewed in 28]. Greer et al. further supported data by providing three-dimensional reconstructions of control and nitrofen-exposed E13.5 rats for a clear visualization of the regional defects within the posterior and caudal regions of the PPF [30].

Subsequent data confirmed an initial PPF defect and went on to implicate amuscular-mesenchymal component of the PPF. Babiuk et al. showed that *C-met* ($^{-}/^{-}$) mice, which have a totally amuscular diaphragm due to the loss of necessary signaling for muscle precursor migration from the somites to peripheral muscles, including the diaphragm, have Bochdalek-type diaphragmatic defects induced by nitrofen with the liver herniating

through the defective mesenchymal sheet [7]. Furthermore, it was demonstrated that in the nitrofen-exposed rat embryos, the mesenchymal substratum in the dorsolateral region of the left PPF, through which the liver was protruding, is missing (figure 1.2) [8].

1.3.5 Summary

In conclusion, what is clear from the above studies is the importance to understand the embryogenesis of the PPF, with an emphasis on the amuscular component, as a major focal point for elucidating the pathogenesis and etiology of CDH.

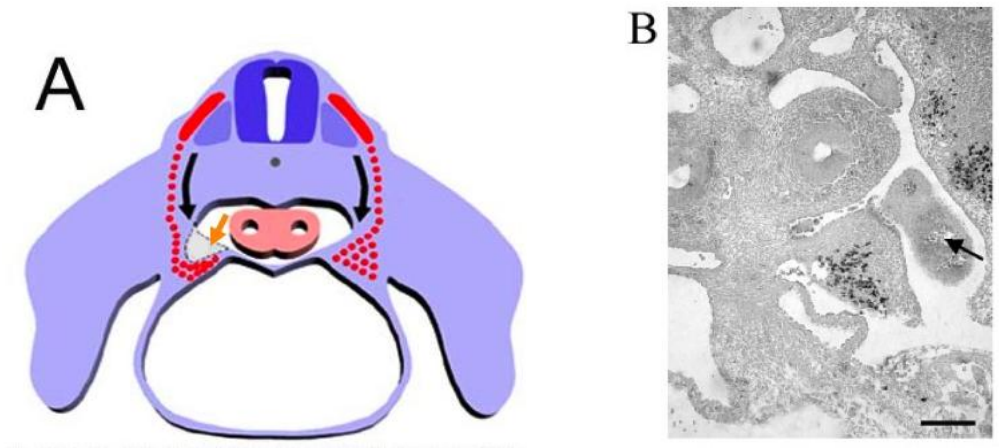

Figure 1.2 Animal model showing basics of the hypothesis that a defect in the mesenchymal substratum of the pleuroperitoneal fold (PPF) underlies CDH pathogenesis.

(A) A schematic representation of a transverse cross-section through a rat embryo showing muscle precursor cells (MPCs) (red) migrating to the triangular-shaped PPF between embryonic day (E)12-E14, from which they later spread to populate the entire diaphragm (E14-E17). In CDH, we hypothesize that a specific region of the dorsolateral PPF is missing prior to MPCs arrival at the PPF (shaded area is missing). Panel (B) is a transverse section of a nitrofen-exposed E13.5 rat embryo showing a malformed left PPF immunolabeled with Pax3/7 for MPCs and the liver herniating through the missing dorsolateral region (arrow). MPCs aggregate in the medial region of the PPF. Scale bar= 100 um (Adapted from Babiuk et al. [8]).

1.4 Embryogenesis of the Amuscular Mesenchymal Component of the PPF

The focus on Wt1 and the developing amuscular component of the PPF in this study is based on four important observations:

(1) Similar PPF malformation in *WT1*-null mutant mice and nitrofen-treated and vitamin A deficient rats

(2) Wt1 does not colocalize with Pax3-positive muscle precursor cells and is thus only expressed in the nonmuscluar mesenchymal component of the PPF as shown by immunohistochemistry

(3) Coexpression of Wt1 and members of the retinoid signaling pathways mainly RALDH2, RARα and RXRα

(4) Coexpression of Wt1 and other CDH associated genes including Fog2, Gata4 and Coup-tfII within cells of the PPF [16; 17; 19]

The *WT1* gene consists of 10 exons spanning 50 kb of genomic sequence. The *WT1* gene product consists of four COOH- terminal C_2H_2 zinc fingers [57; reviewed in 77]. Its NH_2 terminus contains both transcriptional repression and activation domains [reviewed in 77]. Additional motifs are essential for self–association, nuclear localization, and RNA recognition and processing [reviewed in 77]. More than 20 *WT1* gene products are generated by a combination of alternative mRNA splicing, initiation of translation at variable start codons, and RNA processing [57; reviewed in 77].

Wt1 is involved in a number of cell functions during embryogenesis. Extensive in situ analysis has shown that Wt1 is expressed in the

intermediate mesoderm, kidneys, gonads, diaphragm and in a domain in the limbs indicating its role in limiting the domains of chondrogenesis and/or interdigital apoptosis and in the mesothelium as early as E9.5 mice embryos and stage 12 chick embryos [36; 57; 58]. The domains in which Wt1 is expressed suggests that it plays a role in enabling cells to flip between mesenchymal and epithelial cell fates [57].

During early nephrogenesis, Wt1 is expressed at low basal level in the metanephric mesenchyme, mammalian kidney precursor, and is upregulated during mesenchymal condensation to induce epithelial conversion [34].

During early cardiac development, Wt1 is expressed in the mesenchymal proepicardial villi on the cranial surface of the diaphragm in the mouse of E9, and it marks the epithelial epicardial cells that migrate from the proepicardial organ onto the surface of the myocardium [57]. Later the epicardial cells begin to delaminate from the epicardium to form subepicardial mesenchymal cells known as epicardial derived cells (EPDCs) which give rise to coronary smooth muscle cells, perivascular fibroblasts, and intermyocardial fibroblasts [57]. Following terminal differentiation, Wt1 is no longer expressed in these cells [57]. In *Wt1* null mice the epicardium does not form correctly with large gaps in the cranial part and complete absence of the epicardium over the ventral surface of the aorta and the myocardium is thin, a phenotype that resembles RA-depleted and *RXR-alpha* knock-out mice [57; 68]. Furthermore, a recent study performed in normal avian and in quail-to-chick chimeric embryos found that Wt1 and RALDH2 are coexpressed in

EPDCs and become down-regulated as EPDCs differentiate and express lineage-specific markers [68]. They also concluded that the function of Wt1 in myocardial development is to maintain the RA expression to prevent premature differentiation of EPDC [68].

Similarly, in the liver the expression of Wt1 coincides with that of RALDH2 in coelomic epithelium, whose expression is also down-regulated as these cells delaminate and disperse among the hepatoblasts, thereby contributing to the stellate cell population and the sinusoidal endothelium. Furthermore, both *Wt1* and *RXRα*-null mice suffer from liver hypoplasia [35]. Similar to the heart, it has also been concluded that in the liver Wt1 is required to maintain RALDH2 expression for normal development [35].

1.5 Diaphragm Embryogenesis

1.5.1 Overview of Diaphragm-Phrenic Nerve Embryogenesis

The literature in the majority of embryology text-books states that the diaphragm musculature arises as a composite from a number of embryological sources: the septum transversum (of anterior endodermal origin), the PPF, the dorsal (or esophageal) mesentery, and the thoracic body wall [8; 24]. However, data from several studies identified the PPF as the sole source of diaphragmatic musculature [8; 24; 30]. The PPF is a wedge-shaped tissue composed of the fusion of the primordial pleuroperitoneal and pleuroperciardial tissues. This fold tapers medially from the lateral cervical wall into the esophageal mesentery and fuses ventrally with the dorsal aspect

of the liver and septum transversum (figure 1.3) [7; 30]. Subsequently, muscle precursor cells from the dermomyotome of cervical somites and the phrenic nerve that form the neuromuscular component of the diaphragm migrate into the PPF [7; 30]. The PPF becomes a well recognized structure between E12.5 and E13.5 in the rat (gestational period is 21 days) and it is the expansion of these structures that leads to the formation of the diaphragm [7; 30].

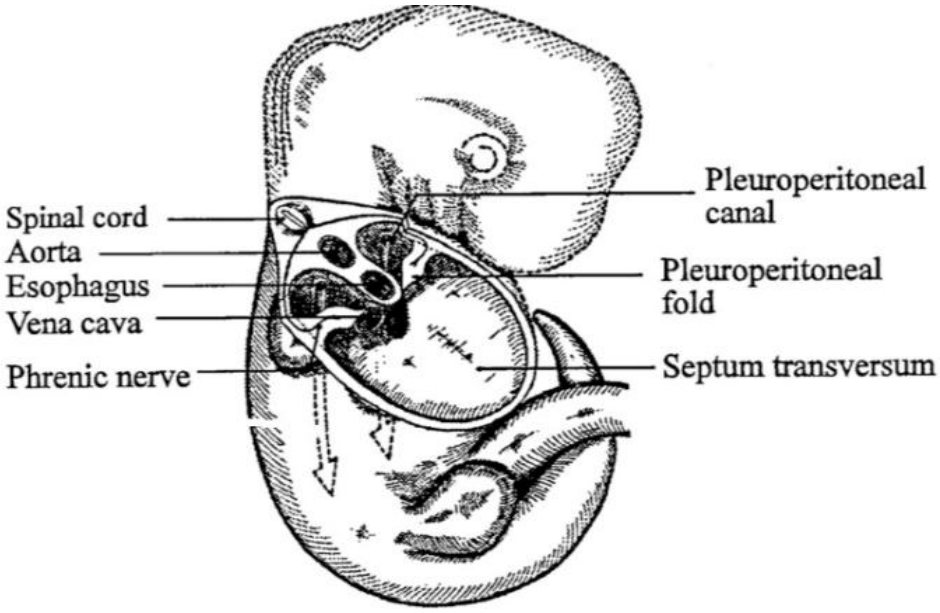

Figure 1.3 Schematic diagram demonstrating the location of the PPF relative to the surrounding tissue.

At E13.5, the triangular shaped PPF extends medially from the lateral body wall to adhere with the esophagus medially and with the septum transversum and the liver ventrally (Adapted from Allan et al. [3]).

Cervical axons emerge from the spinal cord at E11 and migrate dorsoventrally, slightly obliquely, to join the other cervical axons and form the brachial plexus at E12.5 [3; reviewed in 29]. During E12.5-E13, the plexus is at the rostrocaudal level of C6 at the base of the forelimb bud. Subsequently, the two populations diverge as phrenic axons continue to grow ventrally toward the PPF and brachial axons turn laterally to grow into the limb bud [3; reviewed in 29]. A few pioneer cells, p75-receptor and neural cell adhesion molecule (NCAM)-expressing cells, advance ahead of the bulk of phrenic axons that grow along this well defined track of cells into the PPF [3; reviewed in 29]. The cellular composition of the migratory track and the identity of guidance cues has not been determined. By E13.5, phrenic axons reach and converge medially within the PPF (figure 1.4) [3; reviewed in 29]. Subsequently, as the heart and lungs enlarge within the thoracic cavity, the PPF and the contacting phrenic nerve descend caudally to the final position of the diaphragm [3]. By E14.5, branching of the phrenic nerve within the diaphragm and myotube formation had commenced [3; reviewed in 29]. Polysialylated (PSA)-NCAM plays an important role in phrenic axon segregation at the brachial plexus and intramuscular branching by promoting axonal defasciculation [2].

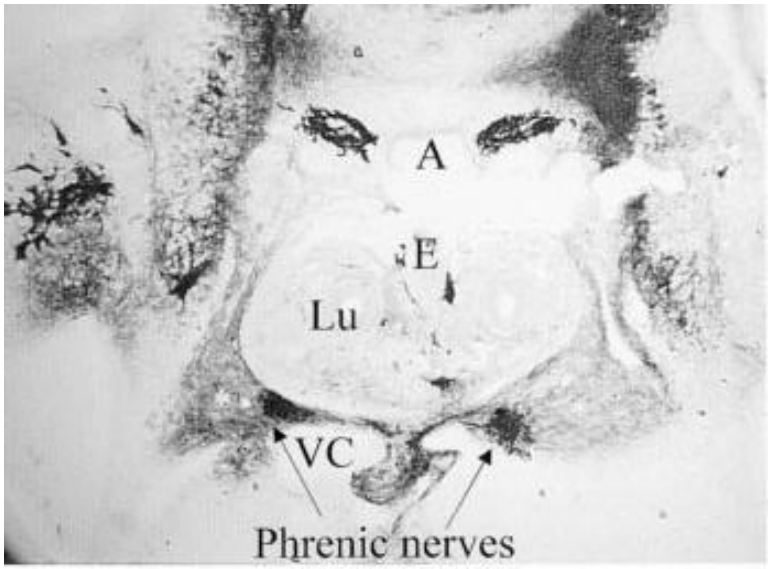

Figure 1.4 The medial location of the phrenic nerve within the PPF.

Transverse section from an E13.5 rat embryo immunolabeled with the low affinity nerve growth factor (p75) receptor for the phrenic nerve and muscle tissue within the PPF. Lu, lung; E, esophagus; A, aorta; VC, vena cava (Adapted from Greer et al. [30]).

Muscle precursor myogenic cells migrate from the cervical somites to the brachial plexus. Subsequently, a subpopulation then continues into the PPF to reach it by E12.5 [reviewed by 49]. The precursor cells then begin to proliferate and differentiate. After E13, there is a radiation of muscle precursors from the PPF towards the dorsolateral costal, sternal costal and crural regions from the centre of these axes to the mediolateral and dorsoventral directions of the diaphragm [2; 8]. By E17, muscle cells have reached all the regions that will be muscularized in the diaphragm, leaving the central tendon and a small tendinous area between the crural and costal regions amuscular [2; 8].

At E14.5, the phrenic nerve in the PPF defasciculates into three intramuscular primary branches which extend in the same three axes as the muscle precursors, into the dorsolateral costal, sternal costal and crural regions of the diaphragm (figure 1.5 A) [2; 3; 8]. At the earliest time of phrenic nerve branching, myoblasts at the point of contact with the nerve began to fuse and form distinct myotubes [2; 3; 8]. As the nerve migrates through the various sectors of the diaphragm, myoblasts along the nerve's path begin to fuse and form additional myotubes [2; 3; 8]. There was always a radiation of myotube elongation from the point of nerve innervation at the centre of the fibers medially toward the central tendon and laterally toward the lateral edge of the diaphragm [2; 8]. These observations are in agreement with the general idea that in all mammalian muscles the end-plate is usually located in the centre of the fiber and that motor axons normally impose regulatory

influences on muscle cells from the point of contact that mediate and facilitate myotube formation via electrically or activity mediated effects [2; 3; 8]. A higher magnification view revealed that the growth cones of phrenic axons lag behind the advancing wave of muscle precursors and developing myotubes by about 200um (figure 1.5 B) [2].

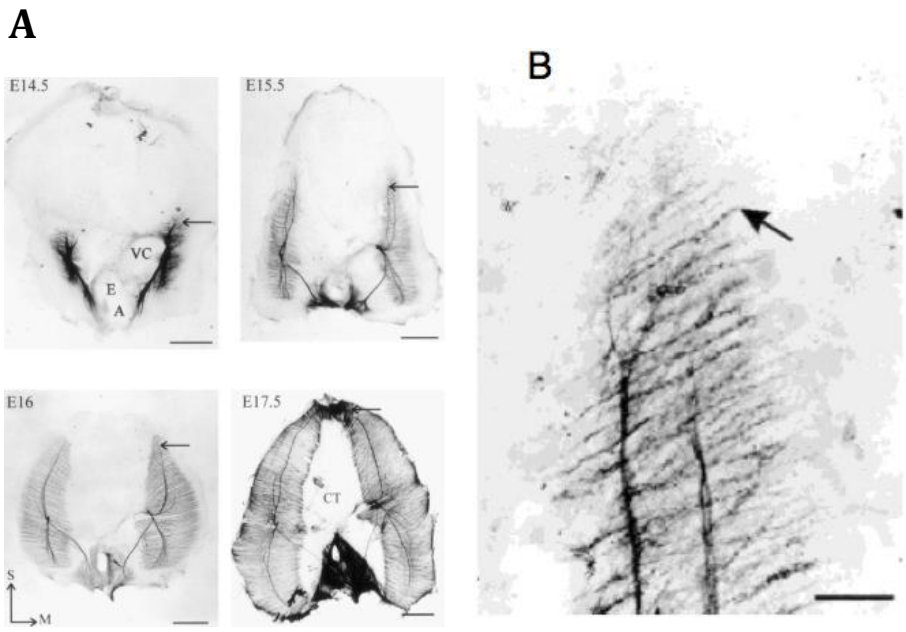

Figure 1.5 Relationship between phrenic nerve intramuscular branching and myotube formation during diaphragm development.

(A) Whole mounts of rat diaphragms isolated at different developmental ages: E14.5 (top left), E15.5 (top right), E16 (bottom left), and E17.5 (bottom right). Phrenic axons and myotubes are immunolabeled with PSA-NCAM demonstrating that during intramuscular branching myotube formation (mediolateral striations) occurs along the nerve's path. (Right sternal branch indicated by arrows). E, esophagus; VC, vena cava; A, aorta; CT, central tendon; S, sternal; M, medial. (B) A higher magnification of an E15.5 rat diaphragm showing primary myotubes ahead of phrenic axons. Scale bars: A= 500 um and B= 100 um (Adapted from Allan et al. [2]).

1.5.2 Summary

Based on what is known so far about diaphragm embryogenesis, there are two basic questions related to nerve-muscle development that require further clarification: (1) what are the cues that guide phrenic axons toward a very localized point within the primordial diaphragm? (2) what determines the characteristic pattern of intramuscular branching within the PPF?

1.6 Schwann Cell Precursor Migration and Axon Interactions

Harrison showed that in *Rana esculenta*, motor axons lacking neural crest cells still followed their normal path to the abdominal myotomal muscles [reviewed in: 62, 63]. This was explained by pointing out that myotomal muscles form close to the ventral root exit zone, so motor axons only have to migrate a short distance to reach them, which they can do without neural crest cells [reviewed in: 62, 63]. However, when their target is further away such as the limbs, motor axons do not migrate in the absence of neural crest cells as seen in Amblystoma[reviewed in: 62, 63]. Many studies have implicated the absence of Schwann cells, which are derived from the neural crest cells as the cause of this failure [62; 63]. A study by Noakes and Bennett demonstrated that in the developing chick forelimb, Schwann cells are located ahead of the main limb nerve and within the early myotube clusters ahead of the nerve branches that innervate the limb muscles [62]. Later, another study by Noakes et al. tested the effects of neural crest removal in the chick embryo, which demonstrated that motor axons reached the base of the limb in the absence of Schwann

cells, but did not enter the limb bud and innervate limb muscles [63]. Furthermore, the motor axons at the base of the limb were scattered and failed to fasciculate and form the main limb nerve trunks [63].

In contrast to the above and in a different study investigating the role of Schwann cells in the guidance of axons during mammalian development, Splotch-mutant mice were used as a genetic model to generate Schwann-cell free lumbo-sacral peripheral nerves in a non-surgical manner [31]. Using light and electron microscopy to visualize the hindlimb nerves, it was observed that despite the absence of Schwann cells the lumbo-scaral nerve trunks and their branches entered the hindlimb in the correct position and contacted the muscle precursor cells, but the cutaneous branches were missing [31].

Furthermore, following a muscle nerve crush and ligations, Schwann cells proliferate at the site of lesion and their associated basal lamina forms bands of Bungner (Schwann cell tubes) that connect proximal and distal regions of the lesion allowing the axons to re-establish their neuromuscular relations [reviewed in 54; 63].

In summary, based on the above studies, it is not clear whether Schwann cells lead axon pathfinding and/or intramuscular branching.

1.7 Guidance Cues that Determine the Pattern of Intramuscular Branching within the Diaphragm

There is always a correlation between phrenic nerve branching and muscle precursor cells that show a greater density along the center of the axes of the diaphragm, around the nerve branches. Furthermore, the growth cones of the phrenic nerve lag behind the migratory muscle cells by about 200um during intramuscular branching [2].

Therefore, muscle precursors could be providing guiding cues to the phrenic axons, whereby Harris (1981) and Lin et al. (2001) demonstrated that there is a concentration of acetycholine receptors (AChR) in the centre of the developing myotubes in the absence of neural innervation, thus providing a target for advancing intramuscular axons, alternatively, common molecular cues from the mesenchymal substratum could provide guidance for migration and proliferation of muscle cells and phrenic axon outgrowth [3; 8; reviewed in: 29, 49].

It has been shown previously that in the absence of muscle cells in chick limb buds following X-irradiation of somitic mesoderm, the main limb nerve trunks and their cutaneous branches formed normally, but the side nerve branches that innervate individual limb muscles were absent [44]. In another study, whereby the somites were removed surgically, it was shown that unlike the previous report, the branches did form in the amuscular chick limb bud, but did not form higher order branches and then degenerated in older embryos [69].

In summary, it appears that muscle cells play a role in establishing and /or maintaining intramuscular branching pattern.

1.8 Summary

CDH is a life-threatening birth defect characterized by a hole in the diaphragm that originates in the amuscular PPF. Regarding PPF embryogenesis and CDH pathogenesis, I determined (1) the embryology of the nerve, muscle and mesenchymal components of the PPF during the critical CDH related period embryonic day (E)12-E14; (2) that the mesenchymal cells of the PPF are of mesodermal origin that undergo epithelial-mesenchymal transformation (EMT) during the critical period of CDH pathogenesis; and (3) in the defective PPF, there is an increase in the density of muscle cells and a decrease in the density of mesenchymal cells.

The phrenic nerve-diaphragm is an excellent model to study the development of the neuromuscular system. My results indicate that phrenic axons and Schwann cells migrate in tandem to the PPF and during the process of intramuscular branching, and that in the absence of migrating muscle precursors, phrenic axons migrate normally to the PPF but intramuscular branching is markedly abnormal.

CHAPTER 2. MATERIALS AND METHODS

2.1 Tissue Collection (Rats and Mice)

Timed-pregnant Sprague-Dawley rats and transgenic mice were housed within the animal breeding facility at the University of Alberta and all experiments were carried out in accordance with the guidelines established by the animal welfare committee at this institution. To obtain pregnant females, animals were set up for overnight breeding. The day in which a morning test reveals the appearance of sperm plugs is designated E0. On the desired day and prior to surgery, rat or mouse dams were anaesthetized with halothane (~3%) using carbogen (95% O_2 and 5% CO_2) as the carrier gas, and maintained at 37°C by radiant heat. A laparotomy was performed to gain access to the abdominal cavity and the gravid uterus and the embryonic and fetal tissue was removed. Embryonic age was confirmed by measuring the crown-rump length (CRL) of the embryos; for rat tissue a previously published growth-curve was used [6]; for mouse tissue we generated our own growth-curve using data from multiple sources [32; 38; 74; 75; 81]. Collected embryos were decapitated, and the hindquarters removed, and the remaining trunk placed in 4% paraforaldehyde (PFA) for fixation for at least 24 hours at 4°C. For fetuses, a dissecting microscope (Leica Wild M3C; Wetzlar, Germany) was used to isolate the whole diaphragm which was then rinsed in phosphate-buffered saline (PBS) and fixed in 4% PFA. To genotype

transgenic mouse tissue, tail and head tissue was removed and frozen immediately.

2.2 Transgenic Mice

2.2.1 Mutant Mice

A full description of how C-met and Pax3-Cre mice were generated has previously been published [9 and 22 respectively].

For genotyping, genomic DNA was isolated from fetal tail or head tissue according to standard protocols. To amplify a 650-bp C-met wild type allele, the following primers were used: WMet8s (5'-CTTTTTCAATAGGGCATTTTGGCTGTG-3') and WMet10 (5'-GTACACTGGCTTGTACAATGTACAGTTG-3'). For the 300-bp C-met mutant allele, the following primers were used: Neo1L (5'-CCTGCGTGCAATCCATCTTGTTCAATG-3') and WMet5 (5'-CACTGACCCAGAAGAGTGG-3'). For the wild-type and mutant bands, the DNA underwent 43 cycles of amplification consisting of denaturing (94°C, 40 s), annealing (65°C, 30 sec), and extension (72°C, 15 sec + 1 sec/cycle). 10 μl of the sample was then run on a 1.2% agarose gel to analyze the results of the PCR reactions.

For Pax3-Cre, the following primers were used: mutant primers (5'-CTG CAC CTA AGG GAC TCC TC-3') and (5'-GTG AAG GCG AGA CGA AAA AG-3') to generate a 190-bp mutant fragment; wild-type primers (5'-AGG CAA

ATT TTG GTG TAC GG-3') and (5'-GTG AAG GCG AGA CGA AAA AG-3') to generate a 169-bp fragment. DNA was amplified for 35 cycles: (30 sec at 94°C, 1 min 65°C, 1min 72°C). Genotyping was performed initially by me, but then by Transnetyx Inc. (a molecular diagnostics company in Memphis, Tennessee) to expedite results.

Wnt1-Cre mice crossed with ROSA line dams were generously provided by Dr. Simon Gosgnach to label neural crest derived Schwann cells. To identify the Wnt1-Cre mice expressing GFP the following primers were used: Cre4 (5'- CAATTTACTGACCGTACAC-3') Cre3 (5'-TAATCGCCATCTTCCAGCAG-3') and eGFP1 (5'-GACGTAAACGGCCACAAGTT-3'); eGFP2 (5'-GAACTCCAGCAGGACCATGT-3'). DNA underwent 2x30 cycles of amplification (1min at 94°C, 1min annealing, 1min at 72°C), followed by 5min at 72°C. Genotyping was performed by Ken Wong, technician in Dr. Gosgnach's lab.

2.2.2 Tie2-LacZ

At E14.5, Tie2-LacZ (Jackson laboratories) embryos were collected and their tails were immediately isolated for genotyping. The isolated tails were rinsed in ice cold X-rinse (2 mM $MgCl_2$, 0.01% sodium deoxycholate, 0.02% Nonidet P-40 in 0.1 M PBS) for 5-10 minutes and then incubated for 4-6 hours in X-gal staining solution (1.0 mg/ml X-gal [5-bromo-4-chloro-3-indyl-β-*D*-galactopyranoside], 2 mM $MgCl_2$, 0.01% sodium deoxycholate, 0.02%

Nonidet P-40, 5 mM potassium ferricyanide, 5 mM potassium ferrocyanide, 20mM Tris).

2.2.3 Mesp1-Cre/R26R

Embryonic tissue from E12 Mesp1-Cre/R26R mice, X-Gal stained and fixed in 4% PFA, were provided by Dr. Iseki from Tokyo Medical and Dental University for immunohistochemistry [51; 76].

2.3 Nitrofen Delivery

On E9.5, timed-pregnant rats were treated via gavage feed with the CDH-inducing compound nitrofen (2,4-dichlorophenyl 4-nitrophenyl ether; obtained from the China National Construction Jiangsu Company [Nanjing, China]. Dams were anaesthetized lightly with halothane and a mixture of 150 mg nitrofen dissolved in 150 ml olive oil was administered.

2.4 Tissue Preparation

Paraffin embedded tissue: Fixed tissue was dehydrated in an ascending series of graded ethanol-water mixtures, dewaxed in xylene and then transferred to plastic moulds containing liquid paraffin for incubation in an oven at 55°C. After ~4 days, the moulds were removed from the oven and the tissue orientated immediately. Serial, transverse sections of paraffin

embedded tissue was then cut using a rotary microtome (Leica RM2135; Leica Microsystems, Wetzlar, Germany) at a thickness of 6 um and mounted on pre-subbed glass slides.

During immunolabeling, sections were dewaxed in xylene and then rehydrated using a graded series of alcohol. Sections were then rinsed in PBS, microwaved in 0.01M sodium citrate buffer, pH 6, at 600 W for 5 minutes before continuing with the immunolabeling protocol.

Whole mount diaphragms: Diaphragms were washed in PBS, immunostained while free floating and then mounted on pre-subbed glass slides.

2.5 Immunolabeling

A list of antibodies used in this study can be found in table 2.1. Note that the concentration of primary antibodies is lower for free floating tissue. Unless stated otherwise, a minimum of three distinct litters were used for each group to confirm the results. All experiments were repeated in triplicate by using three embryos per litter, including negative controls, to confirm the pattern of staining, and representative examples were chosen for presentation.

Immunohistochemistry: Sections were pretreated with 1% hydrogen peroxide in 100% methanol for 30 minutes. Sections were treated with 10%

donkey serum in 0.4% Triton X-100/PBS for 30 minutes before incubation with the appropriate primary antibody. All primary antibodies were diluted in PBS with 1% donkey serum and 0.4% Triton X-100; the antibodies were left to incubate overnight at room temperature. After incubation with primary antibodies two different approaches were used to visualize primary antibody localisation: i) chromogenic visualization and ii) fluorescent visualization (double and triple-labeling).

For chromogenic visualization, sections were thoroughly washed with PBS and incubated with the appropriate biotin conjugated secondary antibody for 60 min at a 1:200 dilution. The slides were then washed in PBS and incubated with a 1:100 avidin-biotinylated peroxidase complex solution (ABC kit, PK4000, Vector Laboratories, Burlingame, CA) for 60 min. A final wash step was followed by antigen visualization via Nickel intensified 3,3-Diaminobenzidine tetrahydrochloride (DAB) labeling (0.04% DAB, 0.04% hydrogen peroxide, 0.6% ammonium nickel sulfate, in 0.1 mol/l Tris buffer) before mounting with Entallen.

For fluorescence, sections were washed with PBS and incubated with the appropriate fluorophore-conjugated secondary antibody (1:200-1:300; with lower concentration for free floating tissue) mixture diluted in PBS and 1% donkey serum albumin for 2 hours. After incubation with the secondary antibody sections were further washed in PBS and coverslipped with Fluorsave mounting medium (Calbiochem, San Diego, CA).

2.6 Microscopy

DAB-labeled tissues were visualized using bright-field microscopy and fluorescent-stained sections were visualized using confocal microscopy. Digital images and figures were prepared for publication using Adobe Photoshop 6.0 (Adobe Systems, Mountains View, CA).

2.6.1 Bright-Field Microscopy

Free-floating tissue was examined and photographed with a bright-field microscope (Leica Wild M3C) attached to a Nikon 990 digital camera (Nikon, Tokyo, Japan). Mounted tissue sections stained with DAB were examined using a conventional optical microscope (Olympus BX40; Olympus corp., Tokyo, Japan) and photographed using the SPOT imaging suite (Diagnostic Instruments, inc.; Sterling Heights, MI).

2.6.2 Confocal Microscopy

Immunostained sections were scanned with a Zeiss Axioplan microscope using an LSM 510 NLO laser configured to a computer running ZEN software (Zeiss, Jena, Germany). For Cy3 fluorescence, excitation (HeNe, 1 mV) was set to 543 nm, and emissions were collected using a 560-nm long-pass filter. For Cy5 excitation (HeNe, 1 mV) was set to 633 nm, and emissions were collected using a 630-nm long-pass filter. For Alexafluor 488 and

fluorescein, excitation (Argon, 40 mV) was set to 488 nm, and emissions were collected with a 505 nm long-pass filter.

2.7 Statistics

In all experiments, the data represents the mean number of cells per unit area ± SEM using student's unpaired t test. The number of sections collected from all animals used for each group was considered as the sample size [n]. The statistical difference was considered to be significant if the p-value was < 0.05. All statistical analyses were performed using Sigma Plot.

Table 2.1- Table of Antibodies used

Antibody	Dilution	Source (Catalogue number)
Mouse antibodies:		
Coup-tfII	1:250	PPMX H7147
MyoD	1: 50	Dako M3512
Wt1	1:50	Dako M3561
GAP-43	1:1000	Sigma 3C11
neurofilament	1:200-1:300	DSHB 2H3
E-cadherin	1:300	BD 610181
Goat antibodies:		
Pax 3/7	1:150-1:300	SCBT 7748
Rabbit antibodies:		
Anti β-galactosidase	1:1000	MP A-11132
N-cadherin	1:1000	AB 12221
Chicken antibodies:		

GFP	1:500	Aves lab GFP-1020

DSHB: Developmental studies hybridoma bank, University of Iowa; SCBT: Santa Cruz Biotechnology; BD: Becton-Dickson Biosciences; AB: Abcam.; PPMX: Persus Proteomics; MP: Molecular Probes.

I treated gavaged animals, isolated the embryos and the diaphragm, performed X-gal staining and the initial genotyping of C-met and Pax3 mutant mice, took and analyzed the light and confocal microscopy photos, did the statistics and prepared the thesis figures.

Immunohistochemistry was performed with the help of Wei Zhang.

CHAPTER 3. RESULTS

3.1 PPF Development in Rodents

In order to study the developing PPF, a series of rat embryos were collected ranging in crown-rump length from 5 mm to 9 mm, which covers an approximate period from E12-E14 (corresponds to gestational weeks 4-6 in human embryos)[rviewed in 16].

There are three components of the PPF that must be differentiated when examining the embryology of the PPF: muscle precursors, the phrenic axons, and the non-muscular component onto which the muscle precursors and nerve migrate.

Recent work by Robin et al. using haematoxylin and eosin staining in combination with immunohistochemical staining with Pax3 for muscle precursor cells (MPCs) and neurofilament for the phrenic nerve (figure 3.1) [18] demonstrated that the MPCs start to be clearly evident within the PPF at~E13 while the phrenic nerve is not yet visible in this structure (figure 3.1 F). Over the next ~36 hours, as the PPF grows in size, a further increase in MPCs is observed with a bundle of neurofilament-positive fibers in a very localized and consistent target within the medial angle of the triangular PPF (figure 3.1 G-H).

The next step was to delineate the relative developmental chronology of the normal amuscular PPF as a basis for its defective formation in CDH. Previous work has determined that the transcription factors Wt1, Coup-tfII, Gata4 and Fog2 are specifically co-expressed in the non-muscular

mesenchymal component of the PPF [19]. Wt1 and Coup-tfII were clearly detected via immunohistochemistry providing the cleanest signal and the mutant mouse models have Bochdalek-type diaphragmatic hernia similar to the nitrofen and vitamin A deficient models [16; 19].

Rat embryos were collected from E12, the earliest age when the PPF is first visualized to E13.5 when it is fully formed. In agreement with previous data, Coup-tfII and Wt1 are expressed in the nuclei of cells throughout the PPF, increasing in number (based on visual inspection) as the PPF develops and grows medially (figure 3.2). Outside the PPF, Coup-tfII positive cells are also found in the adjacent lung mesenchyme; while the expression of Wt1 is more restricted to the mesodermal tissue, the mesothelium (figure 3.2).

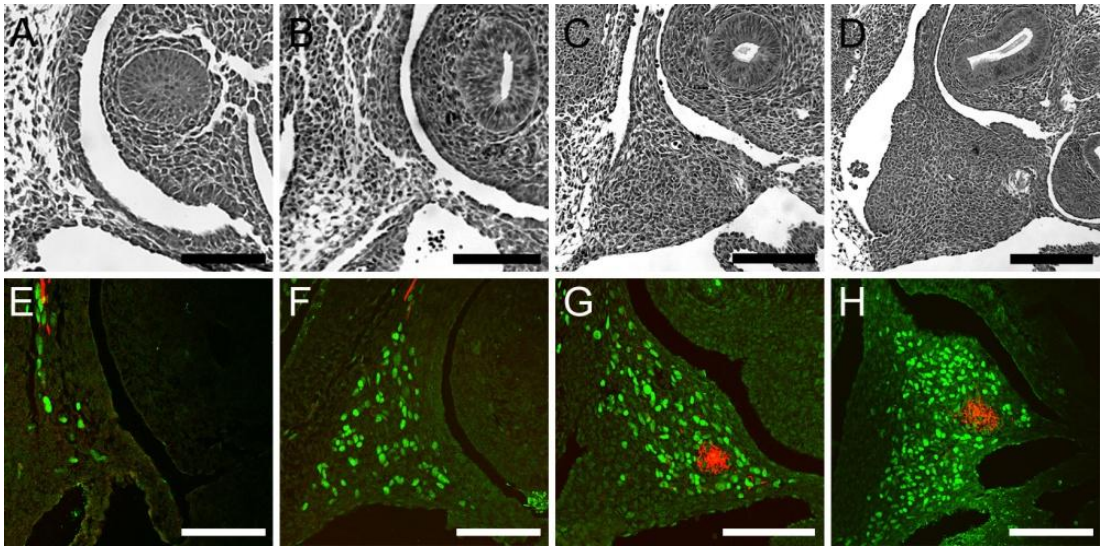

Figure 3.1 Sequential arrival of MPCs and phrenic nerve into the PPF during development.

Hematoxylin-stained transverse sections of the developing PPF from embryonic day E12 (A), E13 (B), E13.5 (C), and E14 (D) rat embryos. The lower row of panels shows a series of confocal microscope images showing immunoflorescence for MPCs (Pax3/7, green) and the phrenic nerve (neurofilament, red) at corresponding ages of E12 (E), E13 (F), E13.5 (G), and E14 (H). Scale bars: A, E = 100 μm; B, C = 150 μm; D = 200 μm; F, G, H = 125 μm (Adapted from Clugston et al. [18]).

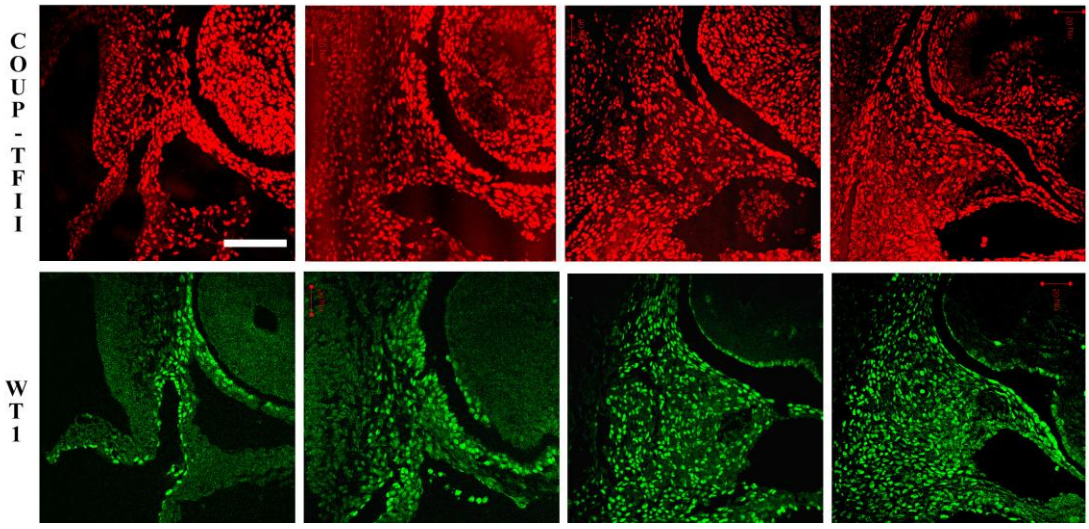

Figure 3.2 Timeline of amuscular PPF development in rat embryo.

Each section shows a column of two single channel confocal images of Coup-tfII (upper channel, red) and Wt1 (lower channel, green) immunolabeling at E12 (A), E12.5 (B), E13 (C), and E13.5 (D) in the PPF. Outside the PPF, Coup-tfII is expressed in the lung mesenchyme, while Wt1 is expressed in the mesothelial cells. Scale bar= 100 um.

3.2 The Origins and Cell Types within the Amuscular Component of the PPF

Given that the amuscular component of the PPF is the focus for understanding the original defect in CDH, it is important to understand the cellular origins and phenotypic transformation of the mesenchymal cells that make up this amuscular substratum. There was very little data in the literature that provide insights into the origins or cellular makeup of the non-muscle component of the PPF.

A previous study in our laboratory tested the neural crest hypothesis using Wnt1-Cre/R26R transgenic mouse model that has a *lacZ* reporter in neural crest derived tissue based on the fact that nitrofen had been shown to target neural crest cells [88]. However, only the Schwann cell precursors surrounding the phrenic nerve within the PPF were labeled [17].

A study by Zhou et al. using $WT1^{CreETR2}$/$ROSA26^{fsLZ}$ to determine the fate of WT1 proepicardial and epicardial cells, showed co-expression of β-gal–positive cells with endothelial cells [83]. Based on this observation, I tested the hypothesis that in the diaphragm, Wt1-mesenchymal cells are derived from endothelial cells using E14.5 Tie2-LacZ transgenic mice, whereby LacZ is expressed in all endothelial-derived cells. However, only vascular endothelial cell were labeled within the diaphragm (data not shown).

Given the fact that Wt1 was expressed in the non-muscle cells of the PPF and that it has been implicated in mesodermal EMT, we tested the hypothesis that amuscular PPF cells are of mesodermal lineage using Mesp1-Cre/R26R transgenic mouse model (embryos from Dr. Sachiko Iseki, Tokyo) that expresses a clearly visible *lacZ* reporter in cells of mesodermal origin. As shown in figure 3.3 A, there was a clear lacZ labeling in the non-muscular Pax3/7-negative PPF cells of E12 transgenic mouse embryos indicative of a mesodermal origin.

We continued investigating the "mesodermal origin hypothesis" by testing the hypothesis that EMT is an important contributor to PPF formation and could be a target for further analyzing CDH pathogenesis. A number of protein markers are typically used to detect various stages of EMT. We initiated our studies by examining the expression of cadherins, cell adhesion molecules known to be important for tissue organization during embryonic development. Specifically, we examined the spatiotemporal distribution of E-cadherin (expressed prior to EMT) and N-cadherin (expressed during and after EMT). As shown in figure 3.3 B, there is a wide-spread N-cadherin expression in the non-muscle cells within the PPF of E13.5 rat and an intense expression of E-cadherin in the mesothelial cells surrounding the PPF. We have not yet studied earlier stages to determine when E-cadherin expression is prominent.

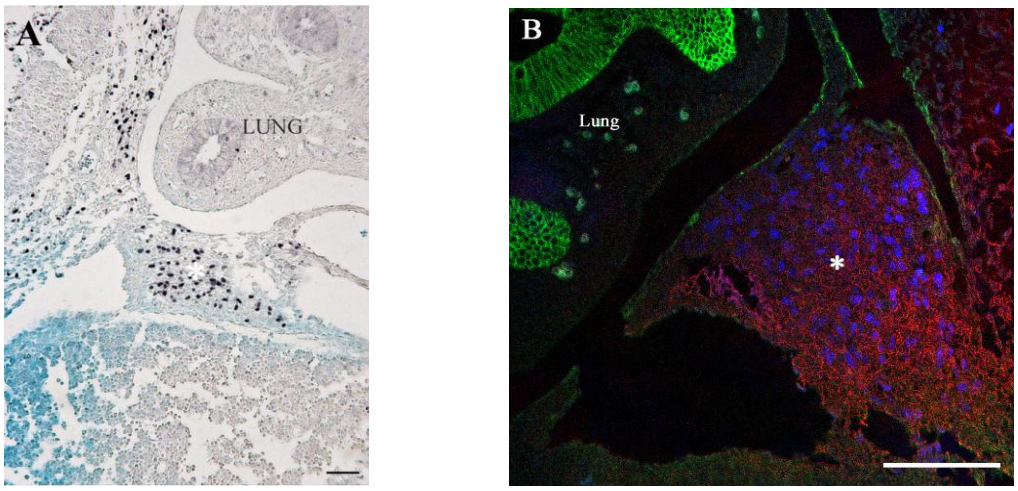

Figure 3.3 Data indicative of mesodermal origin of non-muscle cells that undergo epithelial-mesenchymal transition (EMT) within a fully formed rodent PPF.

(A) Right PPF (*) from an E12 Mesp1-Cre/R26R Lac-Z mouse. The blue deposit in the PPF non-muscle cells is indicative of a mesodermal cell lineage. Brown staining is Pax 3/7 immunolabeling of MPCs. (B) Triple labeling of an E13.5 rat left PPF (*) for Pax 3/7 (blue), E-cadherin (green) and N-cadherin (red). The N-cadherin positive non-muscle cells at this stage, indicative of EMT. E-cadherin is expressed in parts of the lung bud and mesothelial cells (green) that have not undergone EMT. Scale bars= 100 um.

3.3 Characterization of Muscle and Mesenchymal Cells in Defective PPF and Diaphragm

Previous data from the teratogenic, vitamin A deficient and transgenic CDH models in conjunction with examination of human CDH diaphragms, demonstrated a consistant thickening of the diaphragm tissue adjacent to the defect [4; 16]. This led to the hypothesis that muscle cell precursors migrate to a defective PPF mesenchyme and occupy the remaining tissue, thus leading to an increased density of cell distribution. Here, I tested that hypothesis by performing immunohistochemical evaluation of Pax3/7 and Wt1 expression in the muscle precursor cells and mesenchymal cells respectively within the PPF of an E13.5 nitrofen exposed rat embryo model of CDH and then in E18 whole diaphragms in rats exposed to nitrofen. Further, the Wt1 expression data allowed for addressing the secondary question of how the amuscular cells were organized in a defective PPF. Specifically, whether or not amuscular cells were also distributed with a higher density adjacent to the defective area.

The rostral border corresponds to the first serial transverse section with a visible PPF protruding medially from the lateral cervical body wall while the caudal boundary refers to the point at which the PPF is no longer discernable from the underlying liver tissue (figure 3.5 A).

To determine whether there is a difference in the arrangement of Pax3-positive and Wt1-positive cells, three to four embryos from each group

were collected and randomly selected middle and caudal PPF transverse sections, where the defect is always most severe, were used to count the number of cells per unit area. A representative example of the chosen sections from rostral to caudal are shown in figure 3.4 for both control and nitrofen treated rat embryos. Statistical analysis (Student's unpaired t test) showed a significant increase in the density of muscle cells (figure 3.5 B: control= 29 ±3.1246 [n=3]; nitrofen= 41 ±1.4142 [n=5]) and a significant decrease in the density of mesenchymal cells (figure 3.5 C: control= 75 ±8.5 [n=3]; nitrofen= 52.4 ±4.02[n=5]) within the defective PPF regions when compared to control.

To determine how the above results fit into the thickening observed around the defect which reflects the hallmark of CDH pathogenesis, we used random sagittal sections from a normal diaphragm and a diaphragm with a posterolateral hernia (figure 3.7 A, B). The sagittal sections are thicker at the periphery of the hernia compared to control (figure 3.6 A, C). Three to four embryos for each group were used to determine the density of Pax3/7 and Wt1-positive cells at 20X (figure 3.7 A, B) and 40X (figure 3.6 C, D) magnification. As in the defective PPF, statistical analysis (Student's unpaired t test) showed a significant increase in the density of muscle cells (figure 3.7 C: control= 26.6667 ± 0.8819 [n=3]; nitrofen= 39.3333 ± 1.3333 [n=6]) and a significant decrease in the density of mesenchymal cells (figure 3.7 D: control= 42.6667 ± 2.0276 [n=3]; nitrofen= 31.8333 ± 0.4773 [n=6]) around

the diaphragmatic hernia relative to control at 20X magnification. This significant difference in the number of muscle and mesenchymal cells was further confirmed at 40X magnification (figure 3.7 E, F: control muscle cells= 25 ± 0.5774 [n=3]; nitrofen muscle cells= 36.4 ± 3.1718 [n=5] and control mesenchymal cells= 45 ± 2.8868 [n=3]; nitrofen mesenchymal cells= 29 ± 1.9235 [n=5]).

Together, these results confirm that the aggregation of muscle cells around the defect is the cause of the observed thickening. The Wt1 expression data is suggestive of reduced number of mesenchymal cells both in the defective PPF and around the diaphragm defect, perhaps due to a decrease in proliferation or increase in apoptosis.

Normal PPF

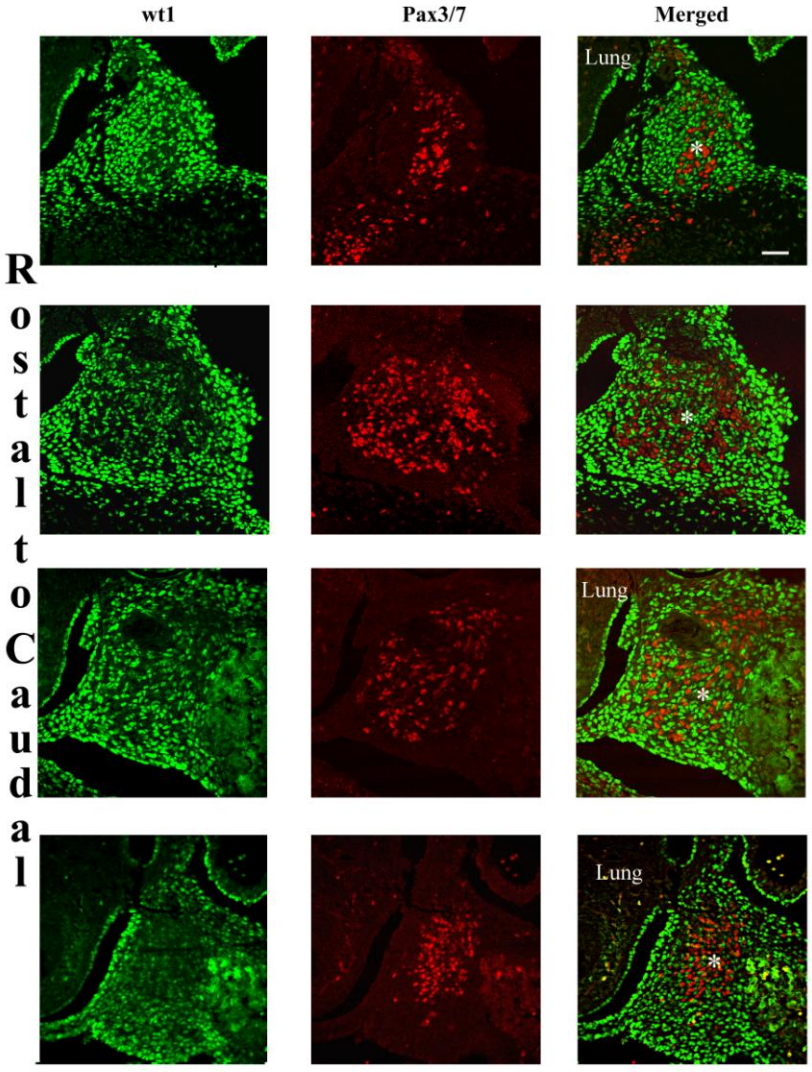

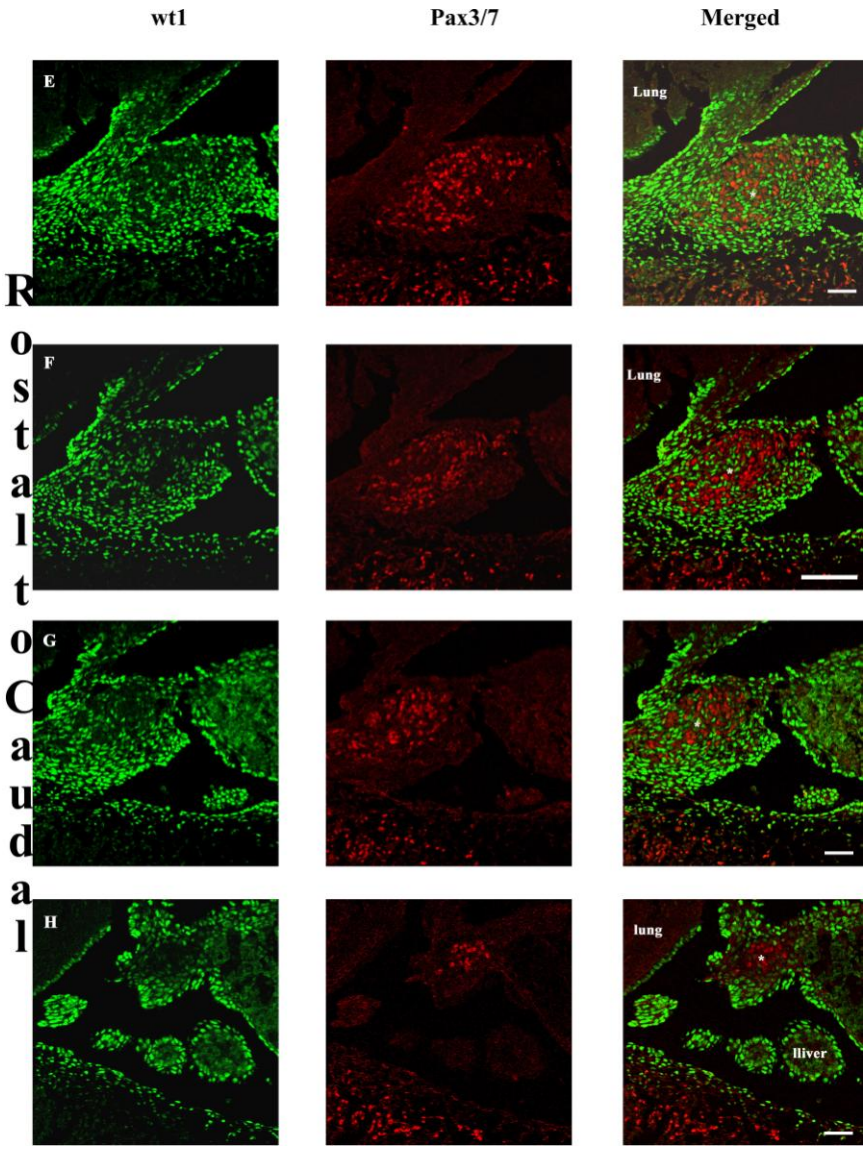

Figure 3.4 Pax3/7 and Wt1 immunolabeling within control and nitrofen-induced right-sided PPF defect at E13.5.

Rostral to caudal (upper to lower panel) series of transverse sections through normal (A, B, C, D) and CDH (E, F, G, H) PPF (*). In each section, the left column shows Wt1-positive non-muscle cells (green), the middle panel shows Pax3/7-positive MPCs (red), and the right panel shows a merged image. Scale bars= 200 um.

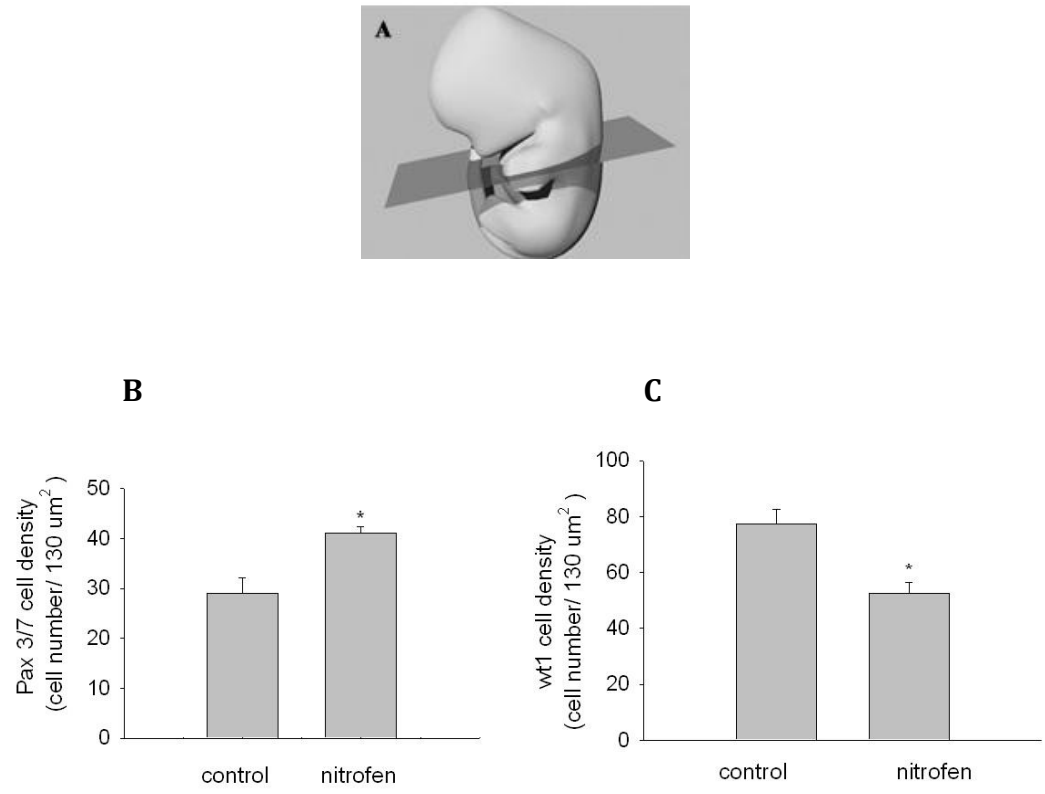

Figure 3.5 Increased MPCs and reduced non-muscle cell density within the nitrofen-model of PPF defect at E13.5.

(A) A transeverse plane at the cervical level of an E13.5 rat embryo. Bar graphs comparing the density of Pax3/7- positive MPCs (B) and Wt1-positive non-muscle cells (C) in the PPF of normal and CDH-PPF. (*) $P < 0.05$ mean $\pm$ SEM.

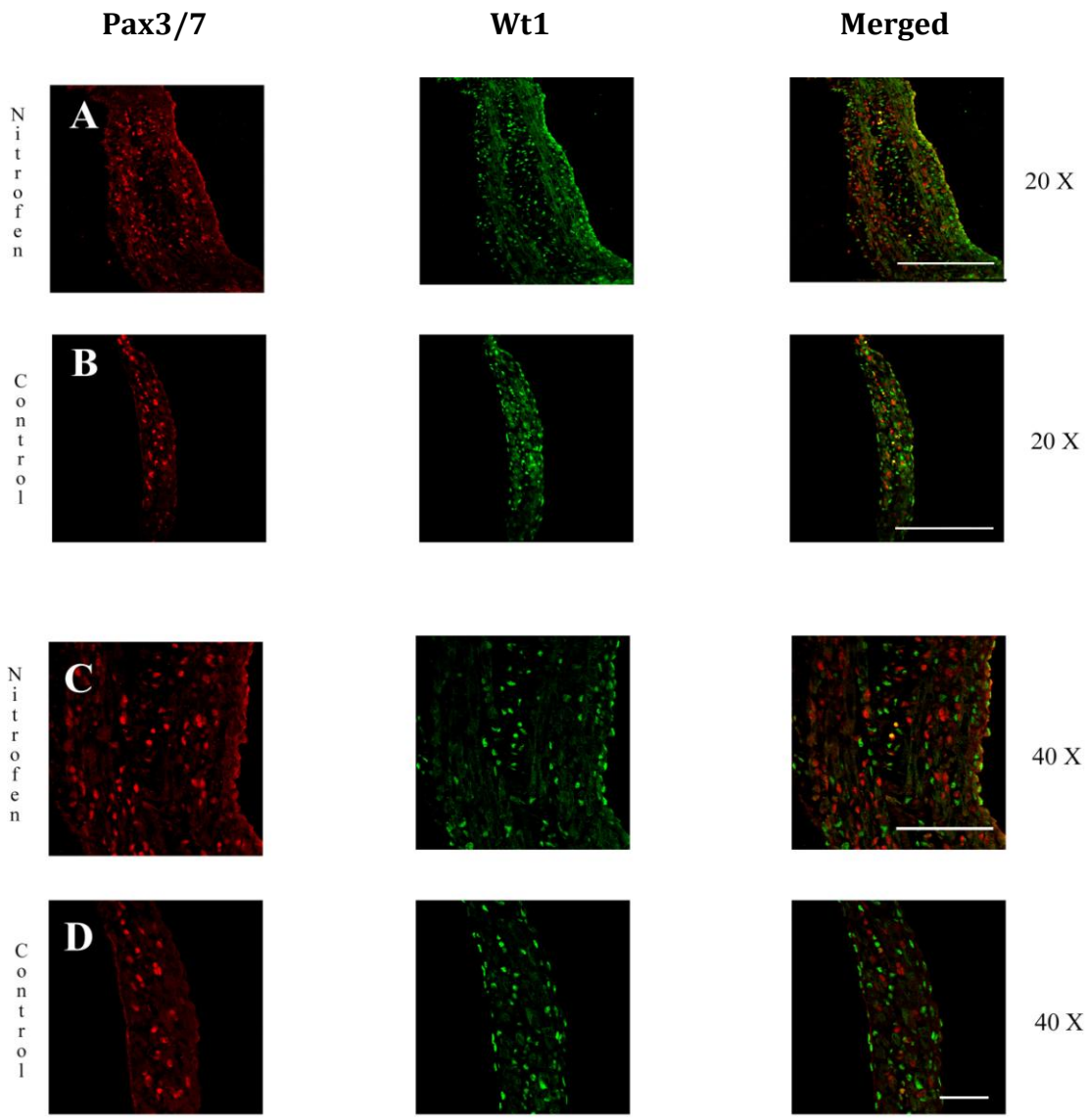

Figure 3.6 Pax3/7 and Wt1 immunolabeling within control and nitrofen-induced diaphragmatic hernia at E18.

Sagittal sections of control (B, D) and defective diaphragm (A, C) at 20 X (A, B) and 40 X (C, D) magnification. In each section, the left column shows muscle cells (Pax3/7, red), the middle column shows non-muscle cells (Wt1, green) and the left column shows merged images. Scale bars: A, B= 200 um, C= 100 um, and D= 50 um.

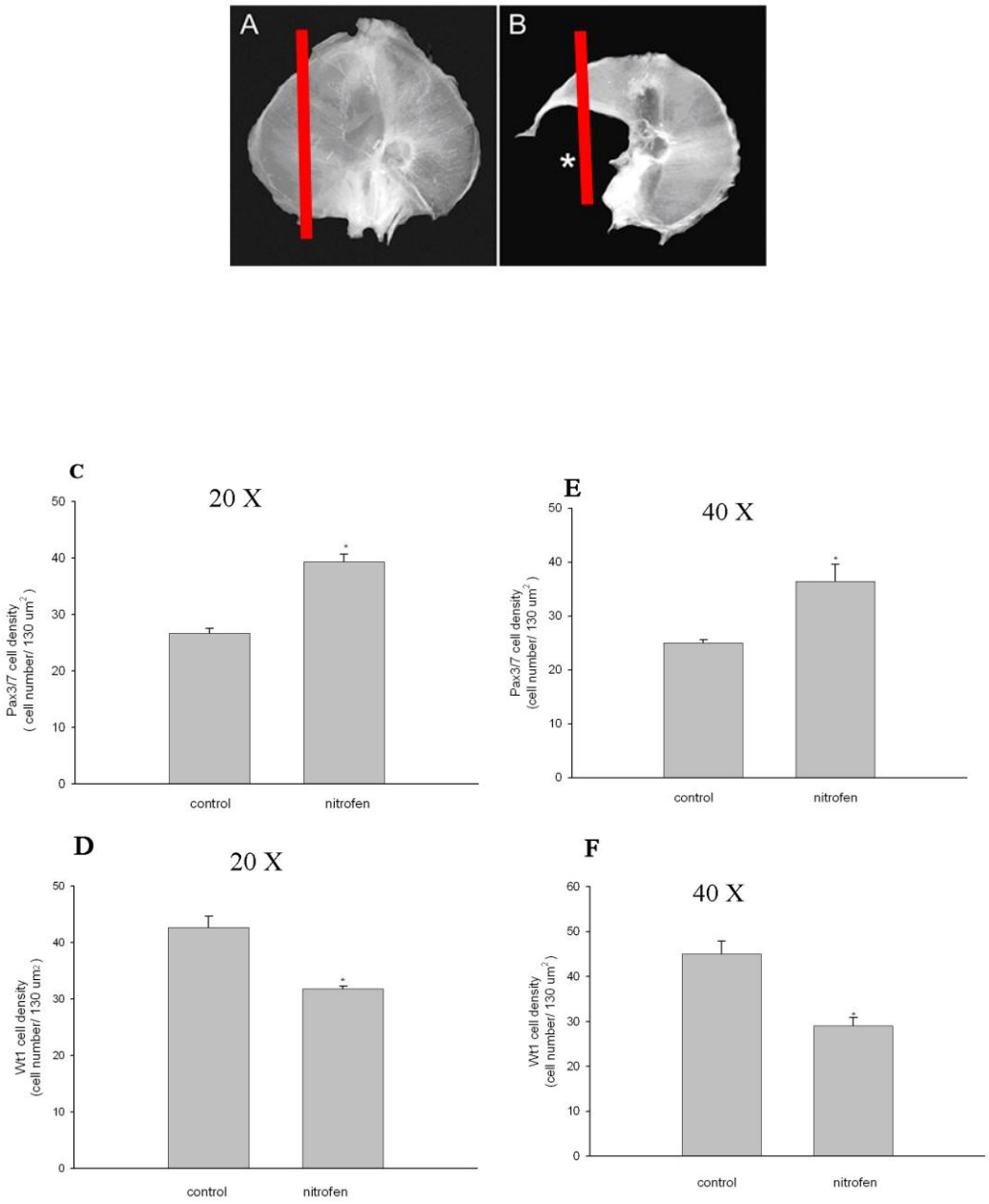

Figure 3.7 Increased MPCs and reduced non-muscle cell density within the malformed diaphragm at E18.

Dashed lines in (A) and (B) demarcate the sagittal plane for both control and malformed diaphragm. Bar graphs comparing the density of MPCs (C, E) and non-muscle cells (D, E) in normal and malformed diaphragm at 20X (C, D) and 40X (E, F) magnification. (*) $P < 0.05$ mean $\pm$ SEM.

3.4 Identification of Schwann Precursor Cells around the Phrenic Nerve during its Initial Migration to the Primordial Diaphragm and during the Process of Intramuscular Branching within the Diaphragm

Previous studies by Allan et al. had demonstrated that phrenic axon growth cones migrate approximately 150-200 um behind migrating muscle precursor cells toward the PPF [2; 3]. Further, growth cones of phrenic nerve intramuscular branches extended a similar distance behind migrating myoblasts and recently formed primary myotubes [3]. As discussed in the next section, this raised questions about the potential interactions between phrenic axon guidance and muscle precursor migration. In addition, as addressed in this section, there was an interest in determining the migration of Schwann cell precursors in relation to the axons and myoblasts.

Our labs previous attempts at examining Schwann cell precursors with immunohistochemical markers were unsuccessful; likely due to poor expression of typical Schwann cell related proteins by early stage precursors. However, I took advantage of Wnt1-Cre mice that when crossed with ROSA line label neural crest derived Schwann cells. Triple labeling of an E10.5 mouse embryo with GFP, GAP-43 and Pax3/7 to delineate Schwann cells and phrenic axons from muscle cells clearly show that a few muscle cells begin to reach the PPF as early as E10.5 while Schwann cells and phrenic axons apparently migrate in tandem to the PPF (figure 3.8 and 3.9 A, D). With further development, the number of muscle cells within the PPF increases as the phrenic nerve and Schwann cells arrive into the PPF surrounded by

muscle precursor cells (figure 3.9 B, C, E, F).

Similarly, double labeling of an E14.5 whole mount diaphragm with neurofilament for phrenic axons and GFP for Schwann cells seems to show the tandem arrival of Schwann cells and phrenic axons during the process of intramuscular branching, although due to the thickness of the tissue, the extent of axon branching is not as clear as within the PPF sections (figure 3.10).

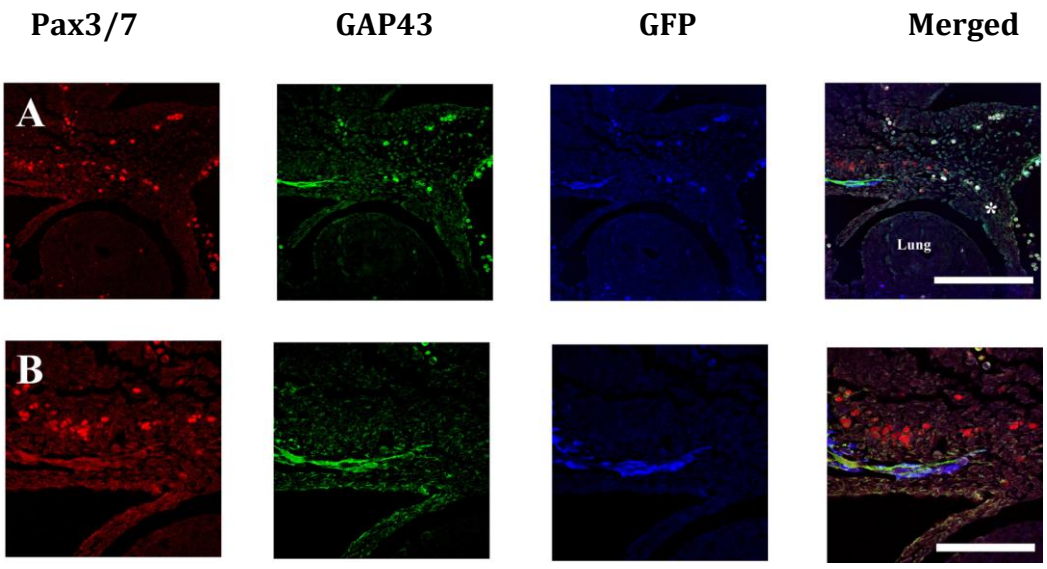

Figure 3.8 Sequential arrival of MPCs, phrenic nerve and Schwann cells into the PPF of E10.5 Wnt1-Cre/ROSA mutant mice.

Triple labeling of left PPF (*) from an E10.5 Wnt1-Cre/ROSA mouse. The top panel shows confocal images at 20X magnification (A), and the bottom panel shows the same images at 40X magnification (B). Each section shows four columns from left to right: MPCs (Pax3/7, red), phrenic nerve (GAP43, green), Schwann cells (GFP, blue) and merged images. Scale bar: A= 200 um, and B= 50 um.

Left PPF

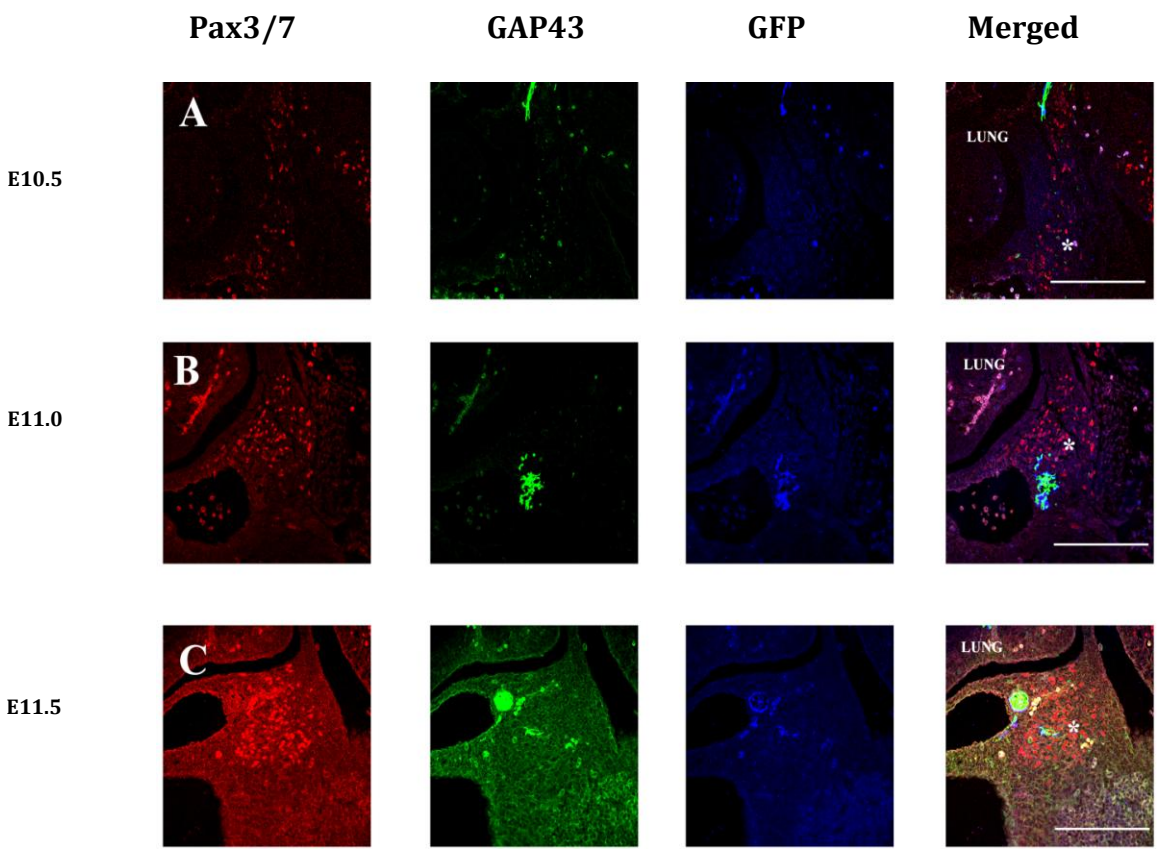

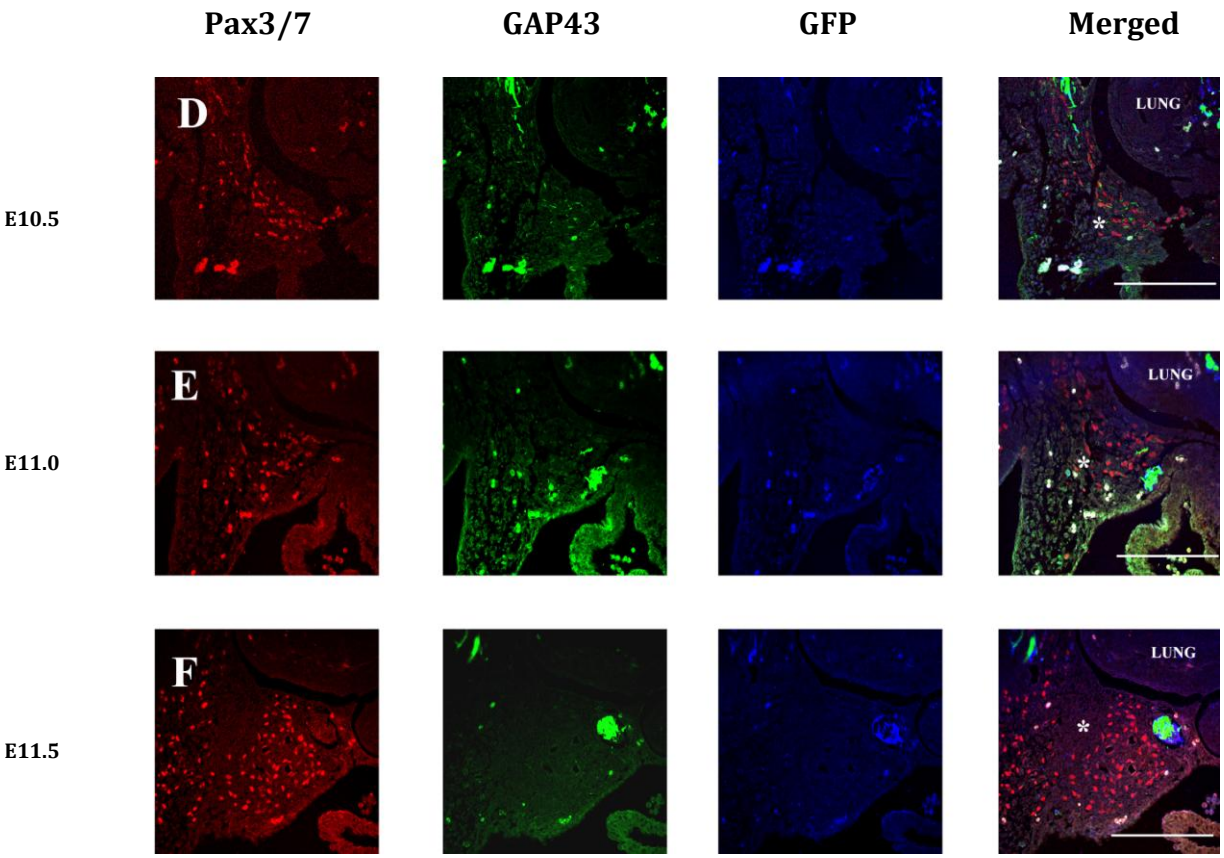

Figure 3.9 The sequential arrival of MPCs, phrenic nerve and Schwann cells into the PPF of Wnt1-Cre/ROSA mice from E10.5-E11.5.

Triple labeling of left (A, B, C) and right (D, E, F) PPF (*) from E10.5 - E11.5 Wnt1-Cre/ROSA mouse. Each section shows four columns from left to right: MPCs (Pax3/7, red), phrenic nerve (GAP43, green), Schwann cells (GFP, blue) and merged images. Scale bars= 200 um.

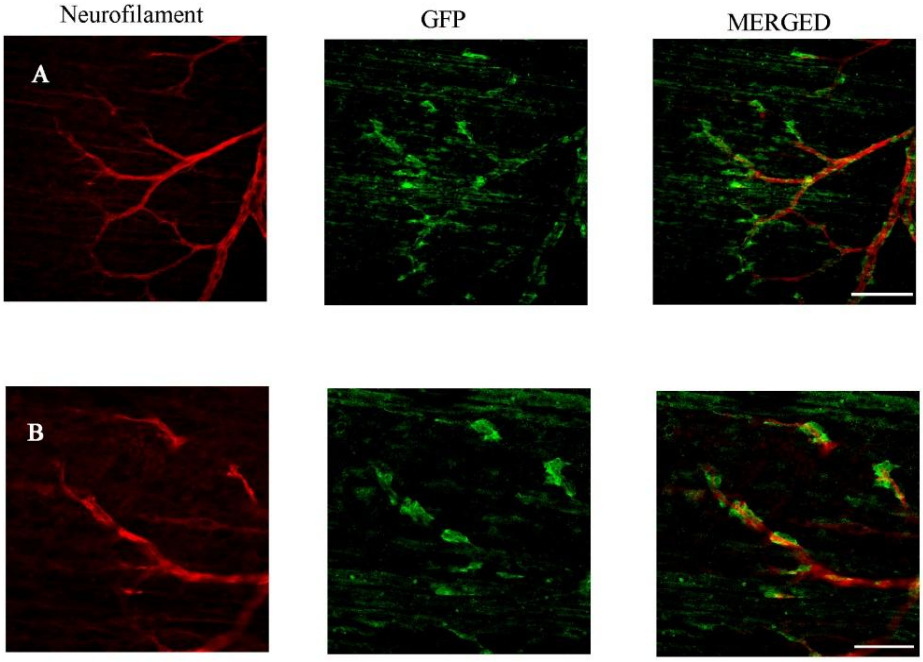

Figure 3.10 Intramuscular branching of phrenic axons within an E14.5 whole mount diaphragm of Wnt1-Cre/ ROSA mice occurs in tandem with the arrival of Schwann cells.

Double labeling of whole mount diaphragm from an E14.5 Wnt1-Cre/ROSA mouse. The top panel shows confocal images at 20X magnification (A), and the bottom panel shows the same images at 40X magnification (B). Each section shows three columns from left to right: phrenic axons (neurofilament, red), Schwann cells (GFP, green) and merged images. Scale bar: A= 200 um, and B=100 um.

3.5 Intradiaphragmatic Branching of Phrenic Axons within Amuscular Diaphragms

Two mutant mouse lines were used to test the hypotheses that in the absence of muscle precursor migration to the PPF, phrenic axon migration to the target area of the PPF and subsequent branching within the diaphragm would be abnormal. Both *C-met* $^{-/-}$ and *Pax3*$^{cre/cre}$ mice have amuscular diaphragms due to loss of signaling necessary for the normal migration of muscle precursors to peripheral muscle, including the PPF. However, *C-met* null mice were used for PPF studies while *Pax3* null mice were used for diaphragmatic studies, since unlike *C-met* null mice which typically do not survive beyond ~E14.5, *Pax3* null embryos survive to term.

In figure 3.11 (A-F), immunolabeling with MyoD for MPCs and neurofilament for phrenic axons demonstrated that in wild type and amuscular PPF, the phrenic axons consistently converge at a position medially within the PPF at E12. In contrast, immunolabeling with neurofilament in an E14.5 amuscular diaphragm demonstrated an abnormal branching pattern within the diaphragm with very few axons compared to control which shows three typical intramuscular branches innervating the sternal, costal and crural regions of the diaphragm (figure 3.11 G-J).

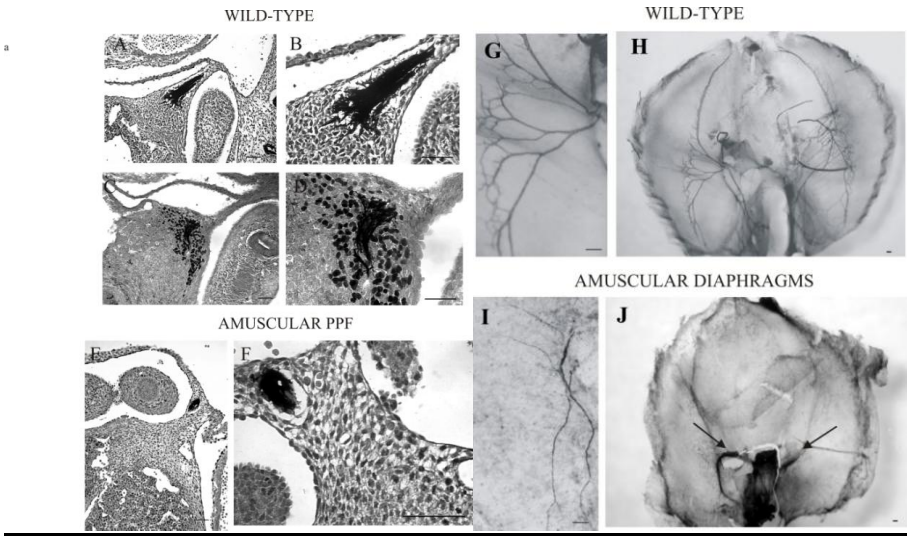

Figure 3.11 The phrenic nerve arrives into the amuscular PPF but has an abnormal pattern of branching within the amuscular diaphragm.

Transverse sections from an E12 wild type (A- D) and C-met mutant mice (E, F) cut at the level of the PPF. The PPF is immunolabeled with either neurofilament only that labels the nerve (A, B) or neurofilament and MyoD to delineate muscle cells (C, D, E, F). Mutant mice show that in the absence of muscle cells, the phrenic nerve enters the PPF at the same medial position as in wild type mice (C, D and E, F). Whole mount diaphragms labeled with neurofilament from E14.5 wild type (G, H) and Pax3/7 mutant mice (I, J). The amuscular diaphragm shows an abnormal intramuscular branching pattern compared to wild type (G and I). Magnifications: A, C= 5X; B, D, F, G, I= 10X; E, H, J= 1.25 X. Scale bars= 100 um.

CHAPTER 4. GENERAL DISCUSSION

4.1 General Discussion

My thesis work addressed both a clinically relevant aspect of diaphragm development with studies of the PPF and basic developmental biology questions pertaining to the interaction of axon pathfinding and myoblast/primordial Schwann cell migration.

4.2 Insights into PPF Embryogenesis and CDH Pathogenesis

Past studies into the pathogenic origin of CDH pointed to the mesenchymal component of the PPF as the primary source of diaphragmatic defect [7; 8]. This notion was supported by Iritani and Kluth et al. who noted a defect in the region of the PPF as early as E13-14 of a nitrofen-treated rat. The same PPF malformation was also found in the vitamin A deficient and *Wt1*-null mouse model [16]. In humans, a similar triangular structure on either side of the body and adjacent to the developing lungs was observed [18]. In addition, as seen in nitrofen and vitamin A deficient models of CDH, there was a thickening of the diaphragmatic musculature around the diaphragmatic defect in humans [16].

Collectively, this relationship between teratogenic and genetic models of CDH and humans with CDH implies that the defect arises from an abnormal PPF. The results presented in the first part of my thesis determined the: (1) precise timing of PPF embryogenesis and the nature of its mesenchymal cells; and (2) pathogenesis of PPF formation in rodents hernias

as it relates to CDH. Data provide a better understanding of the likely timeframe and mechanism of PPF malformation in human cases of CDH.

The data can be summarized as follows. (1) The amuscular component of the PPF forms between E12 and E13.5 when the PPF is fully formed. This corresponds to approximately 4 - 6 weeks in humans. This timeframe is considerably earlier than 8-10 weeks, which is often cited in text-book versions that assume a failure of the diaphragm to fuse with the body wall as being the underlying pathogenic mechanism. (2) The amuscular PPF contains cells of mesodermal origin that undergo EMT; during the stage of PPF malformation in CDH models. Thus, studies of EMT formation are a primary focus of newly established research in the lab. (3) There is an increase in the density of muscle cells in the defective PPF and around the diaphragmatic hernia of nitrofen model of CDH. This explains the thicker diaphragm muscular arrangement in rodent models and human CDH cases. In contrast, the mesenchymal cell density is lower suggesting a primary problem in proliferation, migration and/or apoptosis, areas that will be explored within our laboratory.

4.3 Potential for a Role in Abnormal EMT in the Developing PPF

The expression of *Wt1*, a gene that encodes a zinc-finger transcription factor, is tightly regulated during embryonic development [57; 58]. The gene is expressed in the kidneys, gonads, proliferating coelomic epithelium and the

sub-coelomic epithelial mesenchyme which gives rise to several structures. This pattern of expression implies that *Wt1* plays an important role in mesenchymal to epithelial and epithelial to mesenchymal cell type transition [57; 58].

After the formation of the epicardium, the epithelial layer around the myocardium, a group of cells undergo EMT resulting in the formation of the EPDCs which invade the myocardial tissue and differentiate into coronary smooth muscle cells, coronary endothelium and perivascular and intermyocardial fibroblasts [68]. The colocalization of Wt1 and RALDH2 in avian and mouse epicardium and subepicardial mesenchyme, and the hypoplastic myocardium in RA-depleted and RXRα, RALDH2, *Wt1* knock-out mice collectively suggest that the function of Wt1 in EMT may be mediated by RA signaling pathway [57; 65; 68].

Similarly, a recent study demonstrated reduced expression of RALDH2 in the coelomic epithelial cells around the liver of *Wt1* null mice, which might explain the small liver size observed in those mice [35; 66].

EMT is a process that mediates both normal embryogenesis and tissue repair and disease progression including fibrosis and cancer cell invasion and metastasis [22; 79]. In addition to upregulation of promigratory molecules and extracellular proteases, a critical event in EMT is altered matrix recognition and adhesion which is achieved by the loss of E-cadherin mediated cell-cell contact and the gain of a mesenchymal associated plasma membrane protein

such as N-cadherin, a process known as "cadherin switching" [22; 59]. E-cadherin can be downregulated by Snail and Slug zinc-finger transcription factors. For example, a study using human embryonic stem (hES) cells as a model system to study EMT which occurs during hES differentiation demonstrated an E- to N-cadherin switch associated with an up-regulation of the E-cadherin repressors Snail and Slug proteins which can also function to inhibit apoptosis [22]. Similarly, a study examining EMT in pancreatic carcinoma observed an increase in N-cadherin expression which may be the cause of metastasis [60]. Interestingly, recent work by Tamiya et al. on the role of cell-cell contact on EMT and proliferation of retinal pigment epithelial (RPE) cells observed that the loss of cell-cell contact induced by increased expression of N-cadherin led to increased cell proliferation by transactivation of cyclin-D1 which is a regulatory subunit required for the transition of cells to the S-phase [79].

An insight into the molecular mechanism underlying reduced EPDCs and its derivatives was performed using conditional knock-out mice whose *Wt1* was deleted from epicardial cells [50]. It supported the role of Wt1 in generating EPDCs from the epicardium via EMT through direct transcriptional activation of Snail and transcriptional repression of E-cadherin [50].

Similarly, RA has been shown to sustain the expression of N-cadherin as a mechanism to prevent progression from precartilage condensation to

cartilage nodules [14]. In the heart, N-cadherin null mouse ES (embryonic stem) showed impaired response to all-trans RA mediated cardiomyogenesis [11].

Thus, based on the above mentioned data we can hypothesize that the PPF mesenchymal cells originate from the mesoderm and undergo EMT by a mechanism that requires co-expression of Wt1 and RA to induce the up–regulation of N-cadherin and thus increase cell proliferation. Furthermore, a disruption of any of those components leads to an abnormal proliferation of the amuscular mesenchymal PPF cells which later translates to a hole in the diaphragm with enhanced muscle accumulation around the defect. A systematic study of EMT related markers will be undertaken in our laboratory to test the hypothesis.

4.4 Future Studies of PPF Formation

The data presented in this thesis so far have provided the basic understanding of when and how the PPF develops as well as its pathogenesis when it is fully formed using a nitrofen model of CDH. To better determine the development and mechanism of CDH pathogenesis, it is essential to perform additional studies using both rats and mice for a more definitive determination. The following is an outline of key experiments that can be performed:

(1) The precise timing of the initial PPF defect via immunohistochemical detection of Wt1 and Coup-tfII-positive mesenchymal cells of the PPF at multiple developmental stages.

(2) The potential role of retinoid signaling in the modulation of Wt1 and Coup-tfII expression.

A nitrofen and a vitamin A deficient model of CDH can be used to examine the effects of decreased retinoid levels on Wt1 and Coup-tfII expression pattern within the PPF mesenchyme during E12-13.5 via immunohistochemistry. To complement the protein expression studies, WT1-lacZ transgenic mice can be used to detect *Wt1* activation pattern within the PPF in response to decreased and increased retinoid levels. A colony of WT1-lacZ mice will be generated by our laboratory.

(3) The effect of retinoid signaling on EMT, cell proliferation and apoptosis of mesenchymal cells within the PPF.

We can examine the effect of CDH-inducing teratogens on the expression pattern of E- and N-cadherin during PPF embryogenesis as means of following normal and abnormal EMT. Further, cell proliferation and apoptosis will be determined using BrDU (bromodeoxyuridine) incorporation and terminal uridine deoxynuleotidyl transferase dUTP nick end labeling (TUNEL) respectively in CDH model during E12-E13.5. The use of *C-met* null mouse tissue for the above labeling will provide the advantage of eliminating muscle precursor cells.

(4) The hypothesis that abnormal signaling through the retinoid receptor RARα is of particular importance in CDH etiology. This is based on the observations of restricted expression of RARα in the middle dorsolateral and throughout the whole caudal region of the mesenchymal component of the PPF which reflects the missing region of tissue in the nitrofen model of CDH [17].

A recent study by Clugston et al. demonstrated that the administration of the pan RAR antagonist BMS493 induced a Bockdalek-type CDH in rats [17]. Those data in conjunction with the fact that RARα expression overlaps with the region of the PPF malformed in CDH, I followed up with a study using a specific RARα antagonist. I administered increasing concentrations (5mg/kg, 10mg/kg, 15mg/kg and 20mg/kg) of the RARα antagonist BMS 614 to mice at 12-hour interval from E9-E11. The embryos were collected at E14.5 with no diaphragmatic abnormality (data not shown).

It is possible that the BMS 614 compound was not getting into the embryo sufficiently. I will extend the studies to allow the fetuses to develop to later stages and examine for indications of retinoid signaling perturbations (e.g. craniofacial abnormalities). Alternatively, we subsequently learned that BMS 493 is actually an inverse receptor agonist, whereas BMS 614 is a receptor antagonist [26; 43]. Unlike antagonists which simply inhibit the recruitment of coactivators, an inverse agonist enhances corepressor interaction with nuclear receptors, thus decreasing the basal activity of

unliganded DNA-bound receptors [26; 43]. My current experiments are directed towards comparing the efficiency of the pan RAR inverse agonists BMS 493 and AGN 193109 with the RARα antagonist Ro 41-5253 in inducing CDH in mice.

It will be an important contribution if we can identify another means of inducing CDH in mice. For instance, I attempted to use *Pax3*$^{cre/cre}$ mice that have amsucular diaphragms to more clearly examine the non-muscle cells of the PPF. Based on previous study by Babiuk et al. using *C-met* null mice, I administered a mixture of nitrofen and bisdiamine at different concentrations (nitrofen= 14.5 mg and bisdiamine= 14.5 mg; nitrofen= 14.5 mg and bisdiamine= 12 mg; nitrofen= 14.5 mg and bisdiamine= 10 mg; nitrofen= 14.5 mg and bisdiamine= 7.5 mg) at E8.5 to induce CDH in *Pax3* $^{cre/cre}$ mice [7; 23]. These homozygous mutant mice typically survive until E18 on a mixed (129/Sv X C57 BL/6J) genetic background with a spectrum of abnormalities including severe neural tube and cardiac defects (data not shown) [7; 23]. However, upon mixture administration, no homozygous embryos survived beyond E12.5. The experiments will be repeated when the appropriate drug that targets RAR is determined.

4.5 Diaphragm Embryogenesis

The work presented in the second part of this thesis shows that muscle cells are not required for pathfinding of phrenic axons and that

Schwann cells and phrenic axons arrive together into the PPF as early as E10.5. Once in the PPF, Schwann cells continue to arrive in tandem with intramuscular branches of phrenic axons. The target muscle cells play an important role in establishing and/or maintaining the pattern of intramuscular branching within the diaphragm.

The observation that Schwann cells accompany phrenic axons during their migration into the PPF and as intramuscular branching proceeds within the diaphragm suggests that Schwann cells do not lead during pathfinding. However, there are data showing an important role in motoneuron survival, organization and bundling, and synapse development. First, erbB2 and erbB3 are members of the erbB family of tyrosine kinase receptors that are expressed in Schwann cells and at the neuromuscular junctions (NMJ) of muscle cells [72; 86]. Since, erbB3 has no or little tyrosine activity due to its altered kinase domain, once it binds neuregulin (NRG), it requires the coreceptor erbB2 to transmit the biological activities of NRG [72; 86]. A study using *erbB2* and *erbB3* rescued mice that lack Schwann cells demonstrated a severe loss of motoneurons at the cervical and lumbar levels of the spinal cord at E18.5, which may be due to the heterogeneous identity of motoneurons and thus different sensitivity to trophic factors [86]. The trophic factors maybe provided by differentiating Schwann cells or Schwann cell precursors and could affect motoneuron survival either by providing soluble trophic factors or by direct contact with the axons [86]. Similarly, *erbB3* null mutant mice confirmed motor and sensory neuronal cell death in the absence

of Schwann cells which peaked at approximately E12-E14 and E15-E18 respectively [72].

Second, the intercostal nerves of *erbB2* and *erbB3* mutant mice split into several bundles with disorganized and poorly fasciculated branches [86]. Furthermore, in the absence of Schwann cells the phrenic nerve of erbB2 -deficient mice was severely defasciculated from E12-E14 followed by complete absence of motoneurons after E16.5 [46].

Third, the phrenic axons of erbB2-deficient mice transiently formed synaptic contacts in normal locations within the diaphragm at E14 which maybe explained by the fact the Schwann cells play a role in synapse stabilization by inducing agrin synthesis via some unknown factors that effect neurons and which in turn increases AChR clustering at the neuromuscular junction NMJ [46; 67].

The second intriguing question is whether muscle cells are important for intramuscular branching within the PPF? Comparing the pattern of intramuscular branching within muscular and amuscular PPF and diaphragm, demonstrated that the phrenic nerve reaches the PPF independent of muscle precursor cells which then play an important role in determining the pattern of intramuscular branching.

Synapse formation in the PPF begins as early as E13.5 in a small population of myotubes, so that when the phrenic nerve reaches the myoblast pool in the medial portion of the PPF, axons form synaptic contact

on these cells. This is evident by the observation of AChR clusters colocalized with nerves and their larger size compared with aneural clusters at this age [45].

AChR cluster formation in the central region of the developing myotubes act as a target for the advancing intramuscular axons [reviewed in 8]. This is supported by data from Harrison (1981) and Lin et al. (2001) who demonstrated the presence of concentrated AChR clusters in the centre of myotubes in the absence of innervation [reviewed in 8]. This is in agreement with electrophysiological studies demonstrating that the cervical motoneurons are electrically excitable and can transmit action potentials at E14, the earliest age studied [reviewed in 29, 45]. Another study showed the responsiveness of diaphragm myotubes to agrin, a heparansulfate proteoglycan that is secreted from motor neurons, in the central region at E14.5 [45]. Together these observations indicate reciprocal interactions driving the formation of synapses between neurites and their target cells [45].

The process of AChR aggregation in the central region of developing muscle has received considerable attention. According to neurocentric model of synapse formation, AChR clusters form in response to nerve-derived agrin [45]. This model has been challenged by the myocentric model, whereby AChR clusters form in the central region of the diaphragm independently of motor neurons [33; 45; reviewed in 49]. As a result, it was suggested that postsynaptic specialization is pre-patterned and subsequently refined by the nerve [33]. In

the central region of the diaphragm where the concentrations of muscle specific-kinase (MuSK), an agrin-receptor in muscle, and its downstream signaling molecules are sufficient for MuSK autoactivation and aneural AChR cluster formation [33; 46]. Thus, the probability that a motor neuron will encounter a preformed AChR and become stabilized by activate MuSK in this region is higher than in the adjacent myotube regions with lower MuSK concentration and requiring nerve-secreted agrin, a positively regulating neuronal signal, for activation [33; 45]. However, neurotransmitter secretion acts as negatively regulating/destabilizing signal [33; 45].

Other signals that may play a role in phrenic axon guidance during intramuscular branching are RPTP-α, and RPTP-δ, members of the leukocyte common antigen-related (LAR) subfamily of receptor protein tyrosine phosphatases (RPTP's), since RPTP-α and RPTP-δ double knock-outs lack phrenic nerve branches in the diaphragm [83]. Although the mechanism of LAR-RPTP signal transduction mechanism are not well understood, it has been shown that the extracellular domain of RPTP-α binds skeletal muscle myotube, but the ligand has not been yet identified [83].

4.6 Future Studies of Diaphragm Embryogenesis

The above findings lay the foundation for addressing the following questions:

(1) What is the molecular mechanism that guides the phrenic axons into the PPF? It is striking that the phrenic axons migrate to precisely the same region of the mesenchyme of the PPF. Clearly, there must be a distinct set of guidance cues involved. netrins 1, 3 and 4 are a family of secreted proteins that are structurally related to laminins [70; 71]. During the development of the nervous system, netrins are bifunctional, directing the growth cones of axons to appropriate targets either as attraction or repulsion guidance cues depending on the type of receptors expressed on the cell surface [70; 71]. Attractive effects of netrins is usually mediated via Deleted in Colrectal Cancer (DCC) and neogenin receptors, while repulsive effects are mediated via UNc5a, b, c and d family of receptors that can act as homodimers or heterodimers with receptors such as DCC [70].

It has been demonstrated that mice homozygous for the null mutation in the netrin receptor UNc5c on a C57BL/6J (B6) inbred background die perinatally because of a respiratory distress [12]. When examined, the motor innervation of the diaphragm was severely defective [12]. At E18.5, there was a wide range of abnormalities that varied from a complete absence of innervation to a partial lack of innervation on either the left, the right or both sides of the diaphragm [12]. Furthermore, at its point of contact with the diaphragm, the diameter of the phrenic nerve was reduced with a significant asymmetrical decrease in the number of axons in the B6.C57BL/6J mutant mice [12]. Similar abnormalities were observed in E13.5 mutant mice, confirming that phrenic axons fail to reach the diaphragm during early

embryogenesis. Unlike B6.C57BL/6J mutant mice, B6.Dcc^{-}/$^{-}$, B6. Neo1^{-}/$^{-}$, and B6. Ntn1^{-}/$^{-}$ had normal pattern of diaphragmatic innervation [12].

This can be explained by the functional redundancy of the DCC and neogenin receptors and netrins 1, 3 and 4. It has been shown that netrin 3 is expressed on motor neurons as well as a subpopulation of sensory and sympathetic ganglia neurons and their axons [78]. Furthermore, another in vitro study demonstrated that netrin4 can promote axon outgrowth and that it can bind to netrin 1 receptors namely DCC and UNC5H1 [70].

Determination of coexpression of DCC, neogenenin and UNC5 receptors within the phrenic nerve, and netrins 1, 3 and 4 along the phrenic axons pathway and within the PPF cells will be interesting toward delineating the mechanism of phrenic axonal guidance by the netrin signaling pathway.

(2) Do intramuscular branches form and then degenerate in the absence of muscle cells? And if so, do Schwann cells still accompany the phrenic axons as they branch?

These questions can be answered by collecting the diaphragms of C-met or *Pax3* mutant mice that have amuscular diaphragm, at different stages of development (E14-E15) and double immunolabeling the diaphragms with neurofilament or GAP-43 and S-100 for phrenic axons and Schwann cells respectively, assuming that the Schwann cells express S-100 by that stage of development.

4.7 Summary of Thesis Contribution

The work presented in this thesis provided the first studies toward understanding the embryogenesis of the amuscular mesenchymal substratum of the PPF, the mesenchymal origin of its cells and the potential for EMT related mechanisms as being a foundation for generating new hypotheses toward understanding the pathogenesis and etiology of CDH. In addition, data from my thesis clarified some of the outstanding questions relating axon, Schwann cell precursor and muscle cell migration to the diaphragm, a model neuromuscular system.

REFERENCES

(1) Ackerman KG, Greer JJ. Development of the diaphragm and genetic mouse models of diaphragmatic defects. Am.J.Med.Genet.C.Semin.Med.Genet. 2007 May 15;145C(2):109-116.

(2) Allan DW, Greer JJ. Polysialylated NCAM expression during motor axon outgrowth and myogenesis in the fetal rat. J.Comp.Neurol. 1998 Feb 16;391(3):275-292.

(3) Allan DW, Greer JJ. Embryogenesis of the phrenic nerve and diaphragm in the fetal rat. J.Comp.Neurol. 1997 Jun 16;382(4):459-468.

(4) Allan DW, Greer JJ. Pathogenesis of nitrofen-induced congenital diaphragmatic hernia in fetal rats. J.Appl.Physiol. 1997 Aug;83(2):338-347.

(5) Alles AJ, Losty PD, Donahoe PK, Manganaro TF, Schnitzer JJ. Embryonic cell death patterns associated with nitrofen-induced congenital diaphragmatic hernia. J.Pediatr.Surg. 1995 Feb;30(2):353-8; discussion 359-60.

(6) Angulo Y, Gonzalez AW. The perinatal growth of the albino rat. Anat Rec. 1932; 52:117–137.

(7) Babiuk RP, Greer JJ. Diaphragm defects occur in a CDH hernia model independently of myogenesis and lung formation. Am.J.Physiol.Lung Cell.Mol.Physiol. 2002 Dec;283(6):L1310-4.

(8) Babiuk RP, Zhang W, Clugston R, Allan DW, Greer JJ. Embryological origins and development of the rat diaphragm. J.Comp.Neurol. 2003 Jan 20;455(4):477-487.

(9) Beurskens LW, Tibboel D, Lindemans J, Duvekot JJ, Cohen-Overbeek TE, Veenma DC, et al. Retinol status of newborn infants is associated with congenital diaphragmatic hernia. Pediatrics 2010 Oct;126(4):712-720.

(10) Bladt F, Riethmacher D, Isenmann S, Aguzzi A, Birchmeier C. Essential role for the c-met receptor in the migration of myogenic precursor cells into the limb bud. Nature 1995 Aug 31;376(6543):768-771.

(11) Bugorsky R, Perriard JC, Vassalli G. N-cadherin is essential for retinoic acid-mediated cardiomyogenic differentiation in mouse embryonic stem cells. Eur.J.Histochem. 2007 Jul-Sep;51(3):181-192.

(12) Burgess RW, Jucius TJ, Ackerman SL. Motor axon guidance of the mammalian trochlear and phrenic nerves: dependence on the netrin receptor Unc5c and modifier loci. J.Neurosci. 2006 May 24;26(21):5756-5766.

(13) Chen MH, MacGowan A, Ward S, Bavik C, Greer JJ. The activation of the retinoic acid response element is inhibited in an animal model of congenital diaphragmatic hernia. Biol.Neonate 2003;83(3):157-161.

(14)Cho SH, Oh CD, Kim SJ, Kim IC, Chun JS. Retinoic acid inhibits chondrogenesis of mesenchymal cells by sustaining expression of N-cadherin and its associated proteins. J.Cell.Biochem. 2003 Jul 1;89(4):837-847.

(15) Clugston RD, Greer JJ. Diaphragm development and congenital diaphragmatic hernia. Semin.Pediatr.Surg. 2007 May;16(2):94-100.

(16) Clugston RD, Klattig J, Englert C, Clagett-Dame M, Martinovic J, Benachi A, et al. Teratogen-induced, dietary and genetic models of congenital diaphragmatic hernia share a common mechanism of pathogenesis. Am.J.Pathol. 2006 Nov;169(5):1541-1549.

(17) Clugston RD, Zhang W, Alvarez S, de Lera AR, Greer JJ. Understanding abnormal retinoid signaling as a causative mechanism in congenital diaphragmatic hernia. Am.J.Respir.Cell Mol.Biol. 2010 Mar;42(3):276-285.

(18) Clugston RD, Zhang W, Greer JJ. Early development of the primordial mammalian diaphragm and cellular mechanisms of nitrofen-induced congenital diaphragmatic hernia. Birth Defects Res.A.Clin.Mol.Teratol. 2010 Jan;88(1):15-24.

(19)Clugston RD, Zhang W, Greer JJ. Gene expression in the developing diaphragm: significance for congenital diaphragmatic hernia. Am.J.Physiol.Lung Cell.Mol.Physiol. 2008 Apr;294(4):L665-75.

(20) Costlow RD, Manson JM. The heart and diaphragm: target organs in the neonatal death induced by nitrofen (2,4-dichlorophenyl-p-nitrophenyl ether). Toxicology 1981;20(2-3):209-227.

(21) Doi T, Sugimoto K, Puri P. Prenatal retinoic acid up-regulates pulmonary gene expression of COUP-TFII, FOG2, and GATA4 in pulmonary hypoplasia. J.Pediatr.Surg. 2009 Oct;44(10):1933-1937.

(22) Eastham AM, Spencer H, Soncin F, Ritson S, Merry CL, Stern PL, et al. Epithelial-mesenchymal transition events during human embryonic stem cell differentiation. Cancer Res. 2007 Dec 1;67(23):11254-11262.

(23) Engleka KA, Gitler AD, Zhang M, Zhou DD, High FA, Epstein JA. Insertion of Cre into the Pax3 locus creates a new allele of Splotch and identifies unexpected Pax3 derivatives. Dev.Biol. 2005 Apr 15;280(2):396-406.

(24) Fisher JC, Bodenstein L. Computer simulation analysis of normal and abnormal development of the mammalian diaphragm. Theor.Biol.Med.Model. 2006 Feb 17;3:9.

(25)Gallot D, Marceau G, Coste K, Hadden H, Robert-Gnansia E, Laurichesse H, et al. Congenital diaphragmatic hernia: a retinoid-signaling pathway disruption during lung development? Birth Defects Res.A.Clin.Mol.Teratol. 2005 Aug;73(8):523-531.

(26) Germain P, Gaudon C, Pogenberg V, Sanglier S, Van Dorsselaer A, Royer CA, et al. Differential action on coregulator interaction defines inverse retinoid agonists and neutral antagonists. Chem.Biol. 2009 May 29;16(5):479-489.

(27) Goumy C, Gouas L, Marceau G, Coste K, Veronese L, Gallot D, et al. Retinoid pathway and congenital diaphragmatic hernia: hypothesis from the analysis of chromosomal abnormalities. Fetal.Diagn.Ther. 2010;28(3):129-139.

(28) Greer JJ, Allan DW, Babiuk RP, Lemke RP. Recent advances in understanding the pathogenesis of nitrofen-induced congenital diaphragmatic hernia. Pediatr.Pulmonol. 2000 May;29(5):394-399.

(29)Greer JJ, Allan DW, Martin-Caraballo M, Lemke RP. An overview of phrenic nerve and diaphragm muscle development in the perinatal rat. J.Appl.Physiol. 1999 Mar;86(3):779-786.

(30)Greer JJ, Cote D, Allan DW, Zhang W, Babiuk RP, Ly L, et al. Structure of the primordial diaphragm and defects associated with nitrofen-induced CDH. J.Appl.Physiol. 2000 Dec;89(6):2123-2129.

(31) Grim M, Halata Z, Franz T. Schwann cells are not required for guidance of motor nerves in the hindlimb in Splotch mutant mouse embryos. Anat.Embryol.(Berl) 1992 Sep;186(4):311-318.

(32)Gruneberg H (1943) The development of some external features in mouse embryos. Journal of Heredity 34(3):89-92

(33) Heeroma JH, Plomp JJ, Roubos EW, Verhage M. Development of the mouse neuromuscular junction in the absence of regulated secretion. Neuroscience 2003;120(3):733-744.

(34) Hosono S, Gross I, English MA, Hajra KM, Fearon ER, Licht JD. E-cadherin is a WT1 target gene. J.Biol.Chem. 2000 Apr 14;275(15):10943-10953.

(35) Ijpenberg A, Perez-Pomares JM, Guadix JA, Carmona R, Portillo-Sanchez V, Macias D, et al. Wt1 and retinoic acid signaling are essential for stellate cell development and liver morphogenesis. Dev.Biol. 2007 Dec 1;312(1):157-170.

(36) Ishii Y, Langberg JD, Hurtado R, Lee S, Mikawa T. Induction of proepicardial marker gene expression by the liver bud. Development 2007 Oct;134(20):3627-3637.

(37)Jay PY, Bielinska M, Erlich JM, Mannisto S, Pu WT, Heikinheimo M, et al. Impaired mesenchymal cell function in Gata4 mutant mice leads to diaphragmatic hernias and primary lung defects. Dev.Biol. 2007 Jan 15;301(2):602-614.

(38) Kaufman MH (1995) *The atlas of mouse development*. London, England: Academic Press

(39) Keijzer R, Puri P. Congenital diaphragmatic hernia. Semin.Pediatr.Surg. 2010 Aug;19(3):180-185.

(40) Kling DE, Cavicchio AJ, Sollinger CA, Schnitzer JJ, Kinane TB, Newburg DS. Nitrofen induces apoptosis independently of retinaldehyde dehydrogenase (RALDH) inhibition. Birth Defects Res.B.Dev.Reprod.Toxicol. 2010 Jun;89(3):223-232.

(41) Kling DE, Schnitzer JJ. Vitamin A deficiency (VAD), teratogenic, and surgical models of congenital diaphragmatic hernia (CDH). Am.J.Med.Genet.C.Semin.Med.Genet. 2007 May 15;145C(2):139-157.

(42) Kluth D, Tenbrinck R, von Ekesparre M, Kangah R, Reich P, Brandsma A, et al. The natural history of congenital diaphragmatic hernia and pulmonary hypoplasia in the embryo. J.Pediatr.Surg. 1993 Mar;28(3):456-62; discussion 462-3.

(43) le Maire A, Teyssier C, Erb C, Grimaldi M, Alvarez S, de Lera AR, et al. A unique secondary-structure switch controls constitutive gene repression by retinoic acid receptor. Nat.Struct.Mol.Biol. 2010 Jul;17(7):801-807.

(44) Lewis J, Chevallier A, Kieny M, Wolpert L. Muscle nerve branches do not develop in chick wings devoid of muscle. J.Embryol.Exp.Morphol. 1981 Aug;64:211-232.

(45) Lin S, Landmann L, Ruegg MA, Brenner HR. The role of nerve- versus muscle-derived factors in mammalian neuromuscular junction formation. J.Neurosci. 2008 Mar 26;28(13):3333-3340.

(46) Lin W, Sanchez HB, Deerinck T, Morris JK, Ellisman M, Lee KF. Aberrant development of motor axons and neuromuscular synapses in erbB2-deficient mice. Proc.Natl.Acad.Sci.U.S.A. 2000 Feb 1;97(3):1299-1304.

(47) Maish MS. The diaphragm. Surg.Clin.North Am. 2010 Oct;90(5):955-968.

(48) Major D, Cadenas M, Fournier L, Leclerc S, Lefebvre M, Cloutier R. Retinol status of newborn infants with congenital diaphragmatic hernia. Pediatr.Surg.Int. 1998 Oct;13(8):547-549.

(49) Mantilla CB, Sieck GC. Key aspects of phrenic motoneuron and diaphragm muscle development during the perinatal period. J.Appl.Physiol. 2008 Jun;104(6):1818-1827.

(50) Martinez-Estrada OM, Lettice LA, Essafi A, Guadix JA, Slight J, Velecela V, et al. Wt1 is required for cardiovascular progenitor cell formation through transcriptional control of Snail and E-cadherin. Nat.Genet. 2010 Jan;42(1):89-93.

(51) McBratney-Owen B, Iseki S, Bamforth SD, Olsen BR, Morriss-Kay GM. Development and tissue origins of the mammalian cranial base. Dev.Biol. 2008 Oct 1;322(1):121-132.

(52) Mendelsohn C, Lohnes D, Decimo D, Lufkin T, LeMeur M, Chambon P, et al. Function of the retinoic acid receptors (RARs) during development (II). Multiple abnormalities at various stages of organogenesis in RAR double mutants. Development 1994 Oct;120(10):2749-2771.

(53) Mey J, Babiuk RP, Clugston R, Zhang W, Greer JJ. Retinal dehydrogenase-2 is inhibited by compounds that induce congenital diaphragmatic hernias in rodents. Am.J.Pathol. 2003 Feb;162(2):673-679.

(54) Mirsky R, Jessen KR, Brennan A, Parkinson D, Dong Z, Meier C, et al. Schwann cells as regulators of nerve development. J.Physiol.Paris 2002 Jan-Mar;96(1-2):17-24.

(55) Montedonico S, Nakazawa N, Puri P. Congenital diaphragmatic hernia and retinoids: searching for an etiology. Pediatr.Surg.Int. 2008 Jul;24(7):755-761.

(56) Montedonico S, Nakazawa N, Puri P. Retinoic acid rescues lung hypoplasia in nitrofen-induced hypoplastic foetal rat lung explants. Pediatr.Surg.Int. 2006 Jan;22(1):2-8.

(57) Moore AW, McInnes L, Kreidberg J, Hastie ND, Schedl A. YAC complementation shows a requirement for Wt1 in the development of epicardium, adrenal gland and throughout nephrogenesis. Development 1999 May;126(9):1845-1857.

(58) Moore AW, Schedl A, McInnes L, Doyle M, Hecksher-Sorensen J, Hastie ND. YAC transgenic analysis reveals Wilms' tumour 1 gene activity in the proliferating coelomic epithelium, developing diaphragm and limb. Mech.Dev. 1998 Dec;79(1-2):169-184.

(59) Moreno-Bueno G, Cubillo E, Sarrio D, Peinado H, Rodriguez-Pinilla SM, Villa S, et al. Genetic profiling of epithelial cells expressing E-cadherin repressors reveals a distinct role for Snail, Slug, and E47 factors in epithelial-mesenchymal transition. Cancer Res. 2006 Oct 1;66(19):9543-9556.

(60) Nakajima S, Doi R, Toyoda E, Tsuji S, Wada M, Koizumi M, et al. N-cadherin expression and epithelial-mesenchymal transition in pancreatic carcinoma. Clin.Cancer Res. 2004 Jun 15;10(12 Pt 1):4125-4133.

(61) Nakazawa N, Montedonico S, Takayasu H, Paradisi F, Puri P. Disturbance of retinol transportation causes nitrofen-induced hypoplastic lung. J.Pediatr.Surg. 2007 Feb;42(2):345-349.

(62) Noakes PG, Bennett MR. Growth of axons into developing muscles of the chick forelimb is preceded by cells that stain with Schwann cell antibodies. J.Comp.Neurol. 1987 May 15;259(3):330-347.

(63) Noakes PG, Bennett MR, Stratford J. Migration of Schwann cells and axons into developing chick forelimb muscles following removal of either the neural tube or the neural crest. J.Comp.Neurol. 1988 Nov 8;277(2):214-233.

(64) Noble BR, Babiuk RP, Clugston RD, Underhill TM, Sun H, Kawaguchi R, et al. Mechanisms of action of the congenital diaphragmatic hernia-inducing teratogen nitrofen. Am.J.Physiol.Lung Cell.Mol.Physiol. 2007 Oct;293(4):L1079-87.

(65) Norden J, Grieskamp T, Lausch E, van Wijk B, van den Hoff MJ, Englert C, et al. Wt1 and retinoic acid signaling in the subcoelomic mesenchyme control the development of the pleuropericardial membranes and the sinus horns. Circ.Res. 2010 Apr 16;106(7):1212-1220.

(66) Onitsuka I, Tanaka M, Miyajima A. Characterization and functional analyses of hepatic mesothelial cells in mouse liver development. Gastroenterology 2010 Apr;138(4):1525-35, 1535.e1-6.

(67) Peng HB, Yang JF, Dai Z, Lee CW, Hung HW, Feng ZH, et al. Differential effects of neurotrophins and schwann cell-derived signals on neuronal survival/growth and synaptogenesis. J.Neurosci. 2003 Jun 15;23(12):5050-5060.

(68) Perez-Pomares JM, Phelps A, Sedmerova M, Carmona R, Gonzalez-Iriarte M, Munoz-Chapuli R, et al. Experimental studies on the spatiotemporal expression of WT1 and RALDH2 in the embryonic avian heart: a model for the regulation of myocardial and valvuloseptal development by epicardially derived cells (EPDCs). Dev.Biol. 2002 Jul 15;247(2):307-326.

(69) Phelan KA, Hollyday M. Axon guidance in muscleless chick wings: the role of muscle cells in motoneuronal pathway selection and muscle nerve formation. J.Neurosci. 1990 Aug;10(8):2699-2716.

(70) Qin S, Yu L, Gao Y, Zhou R, Zhang C. Characterization of the receptors for axon guidance factor netrin-4 and identification of the binding domains. Mol.Cell.Neurosci. 2007 Feb;34(2):243-250.

(71) Rajasekharan S, Kennedy TE. The netrin protein family. Genome Biol. 2009;10(9):239.

(72) Riethmacher D, Sonnenberg-Riethmacher E, Brinkmann V, Yamaai T, Lewin GR, Birchmeier C. Severe neuropathies in mice with targeted mutations in the ErbB3 receptor. Nature 1997 Oct 16;389(6652):725-730.

(73) Romeih M, Cakstina I, Zile MH. Retinoic acid is a negative physiological regulator of N-cadherin during early avian heart morphogenesis. Dev.Growth Differ. 2009 Dec;51(9):753-767.

(74) Rugh R (1964) *Vertebrate embryology: the dynamics of development.* New York, USA: Harcourt, Brace and World

(75)Rugh R (1990) *The mouse: its reproduction and development.* Oxford, England: Oxford University Press

(76) Saga Y, Miyagawa-Tomita S, Takagi A, Kitajima S, Miyazaki J, Inoue T. MesP1 is expressed in the heart precursor cells and required for the formation of a single heart tube. Development 1999 Aug;126(15):3437-3447.

(77) Scholz H, Kirschner KM. A role for the Wilms' tumor protein WT1 in organ development. Physiology (Bethesda) 2005 Feb;20:54-59.

(78) Seaman C, Cooper HM. Netrin-3 protein is localized to the axons of motor, sensory, and sympathetic neurons. Mech.Dev. 2001 Mar;101(1-2):245-248.

(79) Tamiya S, Liu L, Kaplan HJ. Epithelial-mesenchymal transition and proliferation of retinal pigment epithelial cells initiated upon loss of cell-cell contact. Invest.Ophthalmol.Vis.Sci. 2010 May;51(5):2755-2763.

(80) Thebaud B, Tibboel D, Rambaud C, Mercier JC, Bourbon JR, Dinh-Xuan AT, et al. Vitamin A decreases the incidence and severity of nitrofen-induced congenital diaphragmatic hernia in rats. Am.J.Physiol. 1999 Aug;277(2 Pt 1):L423-9.

(81) Theiler K (1972) *The house mouse: development and normal stages from fertilization to 4 weeks.* Berlin, Germany: Springer

(82) Toma S, Isnardi L, Raffo P, Riccardi L, Dastoli G, Apfel C, et al. RARalpha antagonist Ro 41-5253 inhibits proliferation and induces apoptosis in breast-cancer cell lines. Int.J.Cancer 1998 Sep 25;78(1):86-94.

(83) Uetani N, Chagnon MJ, Kennedy TE, Iwakura Y, Tremblay ML. Mammalian motoneuron axon targeting requires receptor protein tyrosine phosphatases sigma and delta. J.Neurosci. 2006 May 31;26 (22):5872-5880.

(84) van Loenhout RB, Tibboel D, Post M, Keijzer R. Congenital diaphragmatic hernia: comparison of animal models and relevance to the human situation. Neonatology 2009;96(3):137-149.

(85) WARKANY J, SCHRAFFENBERGER E. Congenital malformations induced in rats by maternal vitamin A deficiency; defects of the eye. Arch.Ophthal 1946 Feb;35:150-169.

(86) Woldeyesus MT, Britsch S, Riethmacher D, Xu L, Sonnenberg-Riethmacher E, Abou-Rebyeh F, et al. Peripheral nervous system defects in erbB2 mutants following genetic rescue of heart development. Genes Dev. 1999 Oct 1;13(19):2538-2548.

(87) You LR, Takamoto N, Yu CT, Tanaka T, Kodama T, Demayo FJ, et al. Mouse lacking COUP-TFII as an animal model of Bochdalek-type congenital diaphragmatic hernia. Proc.Natl.Acad.Sci.U.S.A. 2005 Nov 8;102(45):16351-16356.

(88) Yu J, Gonzalez S, Diez-Pardo JA, Tovar JA. Effects of vitamin A on malformations of neural-crest-controlled organs induced by nitrofen in rats. Pediatr.Surg.Int. 2002 Oct;18(7):600-605.

(89) Zhou B, Ma Q, Rajagopal S, Wu SM, Domian I, Rivera-Feliciano J, et al. Epicardial progenitors contribute to the cardiomyocyte lineage in the developing heart. Nature 2008 Jul 3;454(7200):109-113.

(90) Zile MH. Function of vitamin A in vertebrate embryonic development. J.Nutr. 2001 Mar;131(3):705-708.